Hyperbolic manifolds supporting Arnold diffusion in quasi–integrable systems

Massimiliano Guzzo, Elena Lega, Claude Froeschle

Hyperbolic manifolds supporting Arnold diffusion in quasi–integrable systems

Massimiliano Guzzo
Università degli Studi di Padova,
Dipartimento di Matematica Pura ed Applicata
via Trieste 63, 35121 Padova, Italy
Elena Lega
Observatoire de Nice, Bv. de l'Observatoire, B.P. 4229,
06304 Nice cedex 4, France.
Claude Froeschlé
Observatoire de Nice, Bv. de l'Observatoire, B.P. 4229,
06304 Nice cedex 4, France.

November 13, 2007

Abstract

We provide the numerical detection of the topological mechanism of Arnold diffusion along resonances of quasi–integrable systems in the regime of validity of the Nekhoroshev and KAM theorems. This result is obtained through an investigation of the stable and unstable manifolds of the hyperbolic manifolds of the phase space which are related to the resonances: first, we explain the qualitative features of these manifolds, which appear to be characterized by peculiar 'flower–like' structures; then, we detect different transitions in the topology which are correlated to the changes of the slopes characterizing the dependence of the diffusion coefficient on the perturbing parameter in a log-log scale. We measure a spread of the manifolds, asymptotic to the resonant ones, which is significant to explain diffusion. We also obtain an indirect numerical verification of the exponential decay of the normal form, as predicted by the Nekhoroshev theorem. Precisely, we measured an exponential dependence of the size of the lobes of the asymptotic manifolds through many orders of magnitude of the perturbing parameter.

1 Introduction

Diffusion in generic quasi–integrable systems at small values of the perturbing parameters has been a very studied subject since the pioneering work of Arnold [1]. The proof of the existence of diffusion of orbits for generic systems satisfying the hypotheses of both KAM and Nekhoroshev theorems is still lacking, and consequently there is not full understanding of the mechanisms which possibly produce diffusion. Since [1], many efforts have been done to relate diffusion in phase space to the topology of the so called stable and unstable manifolds of the normally hyperbolic invariant manifolds of the system. This has been done for the so called a priori unstable systems [4], [5], [6], [25],[26], which we studied in [2].

For quasi–integrable systems the situation is more complicated than for the a priori unstable ones for two reasons: first, the quantities related to diffusion decrease exponentially with the perturbing parameter ϵ, so that it is very difficult to measure them numerically; second, the hyperbolic structures are generated by the perturbation, and hyperbolicity disappears when $\epsilon = 0$. Therefore, at any small ϵ, there is the problem of identifying the normally hyperbolic invariant manifolds of the system and to describe the properties of their asymptotic manifolds, which are clearly related to resonances.

The problem we face is the following. In previous papers [18],[19],[20] we have measured diffusion in quasi–integrable systems identified as Arnold diffusion. Using the Fast Lyapunov Indicator method (FLI hereafter, see [11],[12] and the Appendix), we have first obtained very precise computations of the so–called Arnold web of these systems [13], and then [18],[19] we have detected sets of orbits diffusing in the Arnold web with a diffusion coefficient decreasing faster than a power law with respect to a perturbing parameter. As a consequence, we identified the phenomenon as Arnold diffusion. In this paper we investigate numerically the topological mechanism which generates this kind of diffusion, and we compare it with the so–called transition chain mechanism.

To bypass part of the technical problems related to this study we will use as a model problem a quasi–integrable system for which a normally hyperbolic invariant manifold Λ of a given resonance can be explicitly identified at any small $\epsilon \neq 0$. First, we study the diffusion properties of the system near this invariant manifold, then we numerically compare the results with those related to generic resonances.

To do this, we use the numerical methods introduced in [2] to represent the stable and unstable manifolds of 2–dimensional hyperbolic invariant manifolds of the system. We are able to provide a satisfactory global description of the topology of the stable and unstable manifolds. For any fixed value of the perturbing parameter, we find that the topology of the stable (unstable) manifolds present peculiar

flower–like structures which we explain by using a model of weakly interacting resonances. By changing the value of the perturbing parameter, we detect different transitions in the topology which are related to the local predominant resonances. We also measure an exponential decreasing of the size of the lobes of the homoclinic tangle related to the asymptotic manifolds in the single resonances through *many orders of magnitude*. This measure provides an indirect numerical verification of the exponential decay of the normal form, as predicted by the Nekhoroshev theorem for maps ([10], [22], [23]).

The comparison among the topology of the asymptotic manifolds with the diffusion properties in the resonance shows that they are correlated: in section 3 we will show that, by changing ϵ, the topology has transitions which approximately correspond to the changes of the slopes of the diffusion coefficient versus ϵ in the log/log representation; in section 5 we will show that the amplitude of the lobes of the homoclinic tangle decreases exponentially with $1/\epsilon^{1/3}$, and we attribute this scaling to the exponentially decrease of the remainder of the resonant normal form, as in the case of the validity of the Nekhoroshev theorem. These facts provide strong indications of the correlations among the exponentially small remainder of the resonant normal forms around Λ, the topology of the stable/unstable manifolds of Λ and the diffusion coefficient along Λ. However, it will be in section 6 that we will show how the stable/unstable manifolds are directly related to the diffusion along Λ. Precisely, we will explain this mechanism by showing that the unstable manifolds of the points $x \in \Lambda$ are unrolled along the direction of diffusion in the action space, with possible many large oscillations in this direction, but with an average systematic drift. In fact, the oscillations of the unstable manifolds along the direction of diffusion in the action space are similar to the large oscillations that the single orbits do during their Arnold diffusion along Λ, and also in that case we needed to perform averages and filters on the data to show the existence of a very slow diffusion. The existence of a systematic drift of the unstable manifold in the direction of diffusion shows how the diffusion along Λ takes place: given a generic point x in the invariant manifold, the dynamics maps the points in a neighborhood U of x along the unstable manifold of x, and because of the spread of this unstable manifold, the set U spreads in the phase space and some of its points return near the invariant manifold 'far away' from the orbit of x. This is the mechanism that we detect and that is behind the diffusion phenomena that we detected in the papers [18], [19],[20].

As for the a priori unstable case that we studied in [2], we do not directly detect transitions of orbits from stable to unstable manifolds, but this is likely due to the fact that the probability of finding an orbit which passes near selected number of heteroclinic points is very small. The existence of heteroclinic transverse intersections remains a

possible way to prove the spread of the asymptotic manifolds in certain situations.

The paper is organized as follows: in section 2 we define our model problem of quasi–integrable system, and we review its dynamical properties; in section 3 we report the computation of the global structure of the hyperbolic manifolds of the system and we detect transitions in their topology; we explain in section 4 the peculiar topology based on flower–like structures in terms of weakly interacting resonances; in section 5 we detect the exponential decreasing of the lobes of the homoclinic tangle related to the asymptotic manifolds in the single resonances; we report in section 6 the detection of the spread of these manifolds in the action space which is significant to explain Arnold diffusion. We review in the Appendix the Fast Lyapunov Indicator method and its use in the detection of hyperbolic manifolds.

2 A model of quasi–integrable system and its dynamics near resonant invariant manifolds

The notion of normally hyperbolic invariant manifolds was introduced in [3], and we recalled it in [2]. While in the a priori unstable systems there exists naturally a normally hyperbolic invariant manifold, this is not the case for quasi–integrable systems. Of course, hyperbolic manifolds are related to the resonances of the system, but it can be difficult to identify them. To be definite, in this paper we refer to the discrete system used in [19], [20], [21], which is defined by the map:

$$\begin{array}{rcl} \phi : & \mathbb{T}^4 \longrightarrow \mathbb{T}^4 \\ & (\varphi_1, \varphi_2, I_1, I_2) \longmapsto (\varphi_1', \varphi_2', I_1', I_2') \end{array} \tag{1}$$

such that:

$$\begin{aligned} \varphi_1' &= \varphi_1 + I_1 \\ \varphi_2' &= \varphi_2 + I_2 \\ I_1' &= I_1 - \epsilon \frac{\sin \varphi_1'}{(\cos \varphi_1' + \cos \varphi_2' + c)^2} \\ I_2' &= I_2 - \epsilon \frac{\sin \varphi_2'}{(\cos \varphi_1' + \cos \varphi_2' + c)^2} \quad , \end{aligned} \tag{2}$$

where ϵ and $c > 2$ are parameters, and the symplectic structure on $\mathbb{T}^4$ is $d\varphi_1 \wedge dI_1 + d\varphi_2 \wedge dI_2$. The map ϕ has the following invariant manifold:

$$\Lambda = \{(I_1, \varphi_1, I_2, \varphi_2) : \quad \text{such that} \quad (I_1, \varphi_1) = (0, \pi)\} \tag{3}$$

for any value of the parameters. When $\epsilon = 0$ the map is integrable and Λ is not normally hyperbolic. For $\epsilon \neq 0$ the map is quasi–integrable, the manifold Λ is still invariant (as well as the manifold $(I_2, \varphi_2) = (0, \pi)$), but one does not immediately recognize if it is normally hyperbolic, so that we will look for a numerical indication of this fact in section 6.

Let us remark that, by normal form theory, it is possible to show that if ϵ is suitably small then an open subset of Λ is normally hyperbolic. In fact, at any point of Λ the angle φ_1 is resonant, and outside the crossing with the other main resonances it is possible to conjugate with a near to the identity canonical transformation the map ϕ to its normal form ϕ' which is a perturbation (of higher orders with respect to ϵ) of the map:

$$\begin{aligned} \varphi_1' &= \varphi_1 + I_1 \\ \varphi_2' &= \varphi_2 + I_2 \\ I_1' &= I_1 - \epsilon u(\varphi_1') \\ I_2' &= I_2 \end{aligned} \tag{4}$$

where:

$$u(\varphi_1) = \frac{\partial}{\partial \varphi_1} \frac{1}{2\pi} \int_0^{2\pi} \frac{1}{\cos\varphi_1 + \cos\varphi_2 + c} d\varphi_2 \quad .$$

The normal form ϕ' can be obtained with a single step of perturbation theory (such as the ones used in [10]), and moreover the canonical conjugation, where it is defined, has Λ as fixed invariant manifold. The map (4) is decoupled in the product of a constant twist for the variables φ_2, I_2 and a two dimensional generalized standard map for the variables φ_1, I_1. The hyperbolic fixed points of this generalized map $(\varphi_1, I_1) \mapsto (\varphi_1', I_1')$ define hyperbolic invariant manifolds for (4), which remain hyperbolic by adding suitably small perturbations.

It is also possible to go beyond the normal forms constructed by one step of perturbation theory, up to a remainder which is exponentially small with respect to an inverse power of the perturbing parameter, as it is done in the proof of the Nekhoroshev theorem for maps (see [10]). To be more precise, using the normal forms constructed in [10] adapted to the present case, we obtain the following:

Proposition. *There exist constants $K = \mathcal{O}(1/\epsilon^{1/16})$, $\alpha_1 = \mathcal{O}(\epsilon^{7/24})$, $\alpha_2 = \mathcal{O}(\epsilon^{11/48})$ and a near to the identity canonical transformation $\mathcal{C}$ defined on the set $B \times \mathbb{T}^2$, where:*

$$\begin{aligned} B = \{(I_1, I_2) \in \mathbb{T}^2 : \ |I_1| \leq \alpha_1 \ \text{ and } \ |k_1 I_1 + k_2 I_2 + 2\pi k_0| \geq \|(k_0, k_1, k_2)\| \alpha_2 \\ \forall \ \ k = (k_0, k_1, k_2) \in \mathbb{Z}^3 \ \text{ with } \ \|k\| \leq K \ \text{ and } \ k_2 \neq 0\} \end{aligned} \tag{5}$$

which conjugates ϕ to a map generated by the function

$$W'(I', \varphi) = I' \cdot \varphi + \frac{I_1'^2}{2} + \frac{I_2'^2}{2} + \epsilon u(\varphi_1, I') + \epsilon \mathcal{R}(I', \varphi) \quad , \tag{6}$$

where u is a perturbation of higher order with respect to ϵ of

$$u_0(\varphi_1) = \frac{1}{2\pi}\int_0^{2\pi} \frac{1}{\cos\varphi_1 + \cos\varphi_2 + c} d\varphi_2 \quad ,$$

and $\mathcal{R}$ is exponentially small with respect to K.

Let us remark that we do not claim that the exponent $1/16$ related to the exponentially small remainder is optimal (see, for example, the introduction to paper [10]). In section 5 we will use the normal form (6) to explain some properties of the topology of the stable and unstable manifolds of the normally hyperbolic invariant manifold, by obtaining also an indirect numerical verification of the exponential decay of the remainder $\mathcal{R}$ with ϵ.

The invariant manifold Λ is in the resonance: $I_1 = 0$. For this reason this resonance is a special one. However, we did not find in our works a difference in the diffusion properties of this resonance and of the other ones defined by: $(k_1, k_2, k_3) \cdot (I_1, I_2, 2\pi) = 0$, with $k_1, k_2, k_3 \in \mathbb{Z}$. In fact, using the normal forms, one proves that the single resonances related to any (k_1, k_2, k_3) contain normally hyperbolic invariant manifolds, eventually interrupted by the double resonances. The advantage of the resonance $I_1 = 0$ is that the normally hyperbolic invariant manifold has the same expression for any ϵ and that it is diffeomorphic to the torus $\mathbb{T}^2$. For these reasons, in this paper we study predominantly this resonant manifold, but we study also a generic one. Precisely, to compare with the results of the papers [19], [20] we study also the hyperbolic manifolds of the resonance $2I_2 = I_1$.

As we already remarked in paper [2], the dynamics of ϕ restricted to Λ, which is represented by the 2–dimensional standard map:

$$\varphi_2' = \varphi_2 + I_2 \quad , \quad I_2' = I_2 - \epsilon \frac{\sin\varphi_2'}{(\cos\varphi_2' + c - 1)^2} \quad , \tag{7}$$

has no diffusion is ϵ is suitably small. We found (see figure 1) that, approximately for $\epsilon < \epsilon_c \sim 0.002$, the map has invariant KAM tori which bound the possibility of chaotic diffusion, which instead can appear for higher values of ϵ. Therefore, for $0 < \epsilon \leq \epsilon_c$ there is not diffusion on Λ but possibly there is diffusion in a neighborhood of Λ for $\epsilon \neq 0$, which we study numerically by using the techniques introduced in [13], [18], [19], [20], [21]. Specifically:

i) individual orbits in a neighborhood of the invariant manifold indeed spread in the I_2 direction, as it is shown in figure 2;

ii) we measured the diffusion coefficient for $c = 2.1$ and for different values of ϵ. Precisely, we computed the average evolution of the mean squared distance of a set of N orbits from their initial conditions. This quantity turns out to grow linearly with time, the slope giving the diffusion coefficient D. The initial conditions for $N = 100$ orbits are:

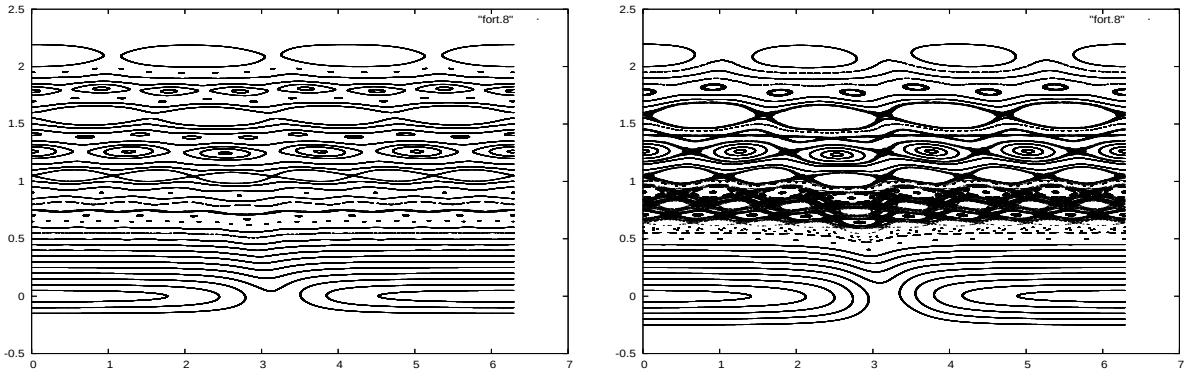

Figure 1: Phase portrait of the restricted map (7) for $\epsilon = 0.002, 0.004$ and $c = 2.1$. On the right panel we see that the region of the phase space with $I_2 \in [0.5, 1]$ is characterized by the overlapping of resonances.

$I_2 = 0.324$, $I_1 \in [-10^{-5}, 10^{-5}]$, $\varphi_1 = \pi$, $\varphi_2 = 0$. According to the results of [18],[19], we found (figure 3) that the diffusion coefficient decreases faster (possibly exponentially) than a power law.

These experimental facts cannot be explained by means of existing rigorous results. Up to now, there is not available any rigorous proof about the existence of diffusion of individual orbits in general cases, even if a quite general result has been announced by Mather [24] in 2003. However, at suitably small ϵ the Nekhoroshev theorem for symplectic maps (see for example [10]) implies an exponential upper bound to the diffusion of orbits, in agreement with the diffusion curve shown in figure 3. We also remark that there does not exist any rigorous result that explains the statistical properties (as the one shown in figure 3, see also [18],[19]) for this kind of diffusion.

3 The global topology of stable and unstable manifolds in a quasi–integrable system

In all our papers [18],[19],[20] we found convenient to study diffusion through two dimensional sections of the phase space, such as:

$$S = \{(I_1, \varphi_1, I_2, \varphi_2) \ \text{ such that } : \varphi_1 = \pi \ \ , \ \ \varphi_2 = 0\} \ . \qquad (8)$$

In figure 2 we represented the spread of orbits with initial conditions in a neighborhood of S. In this section we compute the intersection among the stable and unstable manifolds of Λ with the section S. We first need to recall some notations (already used in paper [2]). For any $x \in \Lambda$ we denote by $W_s^{loc}(x), W_u^{loc}(x)$ (see [3]) the smooth manifolds

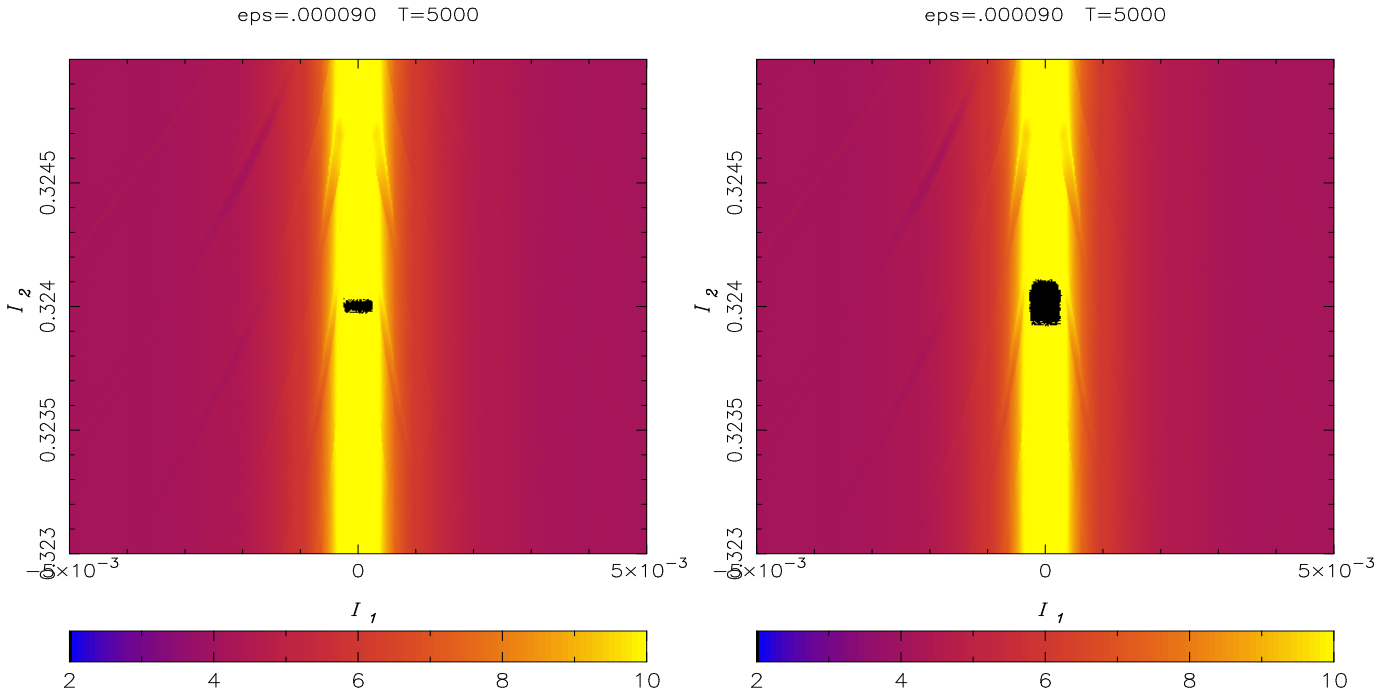

Figure 2: Representation of the FLI for the map (2) with $c = 2.1$ and $\epsilon = 9\,10^{-5}$. For any initial condition with $I_1 \in [-0.005, 0.005]$, $I_2 = [0.3235, 0.3245]$ we plot the value of the FLI after 5000 iterations of the map using a color scale. The black points on the FLI figure represent the points of the orbits of $N = 100$ initial conditions with $I_1 \in [-10^{-5}, 10^{-5}]$, $I_2 = 0,324$, $\varphi_1 = \pi$, $\varphi_2 = 0$ which re-enter in the neighborhood of the surface $S = \{(I_1, \varphi_1, I_2, \varphi_2)$ such that : $\varphi_1 = \pi \quad , \quad \varphi_2 = 0\}$ defined by $|\varphi_1 - \pi| + |\varphi_2| \leq 0.05$. In the left panel the orbits are computed up to $2\,10^7$ iterations, in the right panel up to 10^9 iterations.

such that: $x \in W_s^{loc}(x), W_u^{loc}(x)$, $T_x W_s^{loc}(x) = E^s(x)$, $T_x W_u^{loc}(x) = E^u(x)$ and for any $n \geq 0$ it is:

$$y \in W_s^{loc}(x) \quad \Rightarrow \quad d(\phi^n(x), \phi^n(y)) \leq C(\mu_1 + c)^n d(x, y)$$

$$y \in W_u^{loc}(x) \quad \Rightarrow \quad d(\phi^{-n}(x), \phi^{-n}(y)) \leq C(\lambda_3 - c)^{-n} d(x, y)$$

with $C, c > 0$ suitable constants (c suitably small) and $d(\cdot, \cdot)$ denotes a distance on M. The stable and unstable manifolds $W_s(x), W_u(x)$ of the point x are then obtained by iterating the local manifolds $W_s^{loc}(x), W_u^{loc}(x)$ with ϕ^{-1} and ϕ respectively.

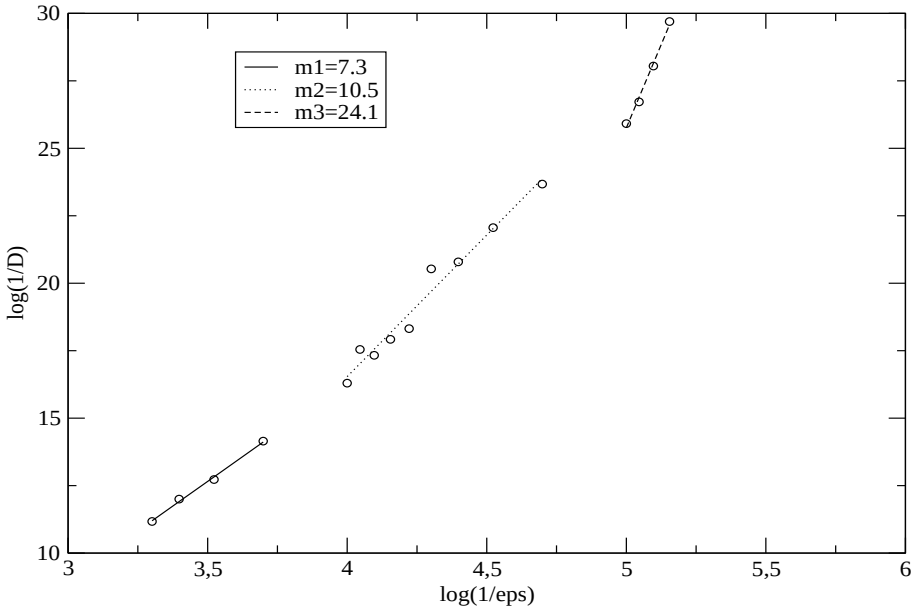

Figure 3: Variation of the diffusion coefficient as a function of ϵ, for $c = 2.1$. Data are well fitted by three different power law $D(\epsilon) \simeq \epsilon^m$ with respectively $m1 = 7.3$, $m2 = 10.5$ and $m3 = 24.1$ in agreement with Nekhoroshev's theorem.

The local stable and unstable manifolds of Λ are defined by:

$$W_s^{loc} = \cup_{x\in\Lambda} W_s^{loc}(x) \quad , \quad W_u^{loc} = \cup_{x\in\Lambda} W_u^{loc}(x) \quad , \tag{9}$$

while the stable and unstable manifolds of Λ are:

$$W_s = \cup_{x\in\Lambda} W_s(x) \quad , \quad W_u = \cup_{x\in\Lambda} W_u(x) \quad , \tag{10}$$

We denote by:

$$S_u^* = \cup_{x\in\Lambda}\Big(S \cap W_u(x)\Big) \quad , \quad S_s^* = \cup_{x\in\Lambda}\Big(S \cap W_s(x)\Big) \quad .$$

the intersection among S and the stable and unstable manifolds of Λ. Let us remark that any invariant torus of $\phi_{|\Lambda}$ intersects S_u^* in only one point x, so that the set S_u^* represents the set where points with initial conditions in a neighborhood of S can return near S following diffusion paths defined by the unstable manifolds of points of Λ.

Transitions in the topology of S_u^*, S_s^*

As we did in [2] we use the FLI method to study the topology of the sets S_u^*, S_s^*. The first set of numerical experiments concerns the map (2) with $c = 2.1$ and different values of ϵ from $\epsilon = 6\ 10^{-6}$ up to $\epsilon = 4\ 10^{-4}$. The results of the computations are reported in figure 4.[1] Precisely, for each value of ϵ we computed the FLI on a grid of 1000×1000 points of S regularly spaced in $-10^{-4} < I_1 < 10^{-4}$, while the action I_2 is in suitable neighborhoods of $I_2 = 0.324$. The FLI is computed up to $T = 5000$ iterations (top panels of figure 4), $T = 2500$ (bottom left panel of figure 4) and $T = 600$ (bottom right panel of figure 4). We recall that the points of the grid which have the highest values of the FLI are those points whose orbit approaches an hyperbolic invariant manifold within the time T, because the growth of tangent vectors is bigger near the hyperbolic manifolds. Therefore, a short–time computation of the FLI allows one to detect a neighborhood of a finite piece of the stable manifold (for the unstable manifold one repeats the computation using the inverse map). The details concerned with this method of computation of the stable and unstable manifolds are discussed in detail in paper [2].

In all the pictures the yellow line at $I_1 = 0$ represents the normally hyperbolic invariant manifold Λ. Around Λ we observe also the presence of peculiar structures related to the dominant resonances, that we will explain in section 4. Here, we remark that these structures are made by different petals centered at crossings of Λ with other resonances. Moreover, we observe that at different values of ϵ the dominant structures which characterize the topology of the stable manifolds are different, according to the local dominant resonances. In fact, for $\epsilon = 6\ 10^{-6}, 10^{-5}$ (top panels of figure 4) we detect two independent sets of petals centered around two resonances which are located just outside the upper side and the lower side of the picture. For $\epsilon = 4\ 10^{-5}$ (figure 4, bottom left panel) the two structures have increased their size with respect to the previous cases, so that their petals overlap in the central part of the picture. For $\epsilon = 4\ 10^{-4}$, one of these structures dominates now the topology of this portion of the action plane, and the other resonances (the horizontal lines) produce only slight modification of the main petals.

These transitions in the topology of the stable manifold are clearly related to the local dominant resonances, which are different at different values of ϵ. This fact can be related to the construction of the resonant normal forms in the proof of the Nekhoroshev theorem. In

[1] The color version of all figures can be found on the electronic version of the paper so that light gray corresponds there to yellow and darker grey corresponds there to red–violet. To better appreciate the topology we uploaded high resolution pictures available also at *http://www.obs-nice.fr/elena/diffusion*. In the final version of the paper the pictures should be available on-line as supplemental material.

fact, in the proof of the Nekhoroshev theorem, different domains of the action space are considered related to different resonances according to the value of a parameter K, which is of the order of an inverse power of ϵ. We also observe that these transitions in the topology of the stable manifold are correlated to the changes of the slopes characterizing the dependence of the diffusion coefficient on ϵ in a log-log scale, shown in figure 3. In fact, $\epsilon = 6\ 10^{-6}, 10^{-5}$ are in the interval characterized by $D(\epsilon) \sim \epsilon^{m3}$, $\epsilon = 4\ 10^{-5}$ is in the interval characterized by $D(\epsilon) \sim \epsilon^{m2}$ and $\epsilon = 4\ 10^{-4}$ is in the interval characterized by $D(\epsilon) \sim \epsilon^{m1}$. Therefore the intervals characterized by a given slope correspond approximately to the different resonances dominating the topology of the stable manifold.

A second set of numerical experiments concerns instead the map (2) with $c = 4$ and a neighborhood of the resonance $2I_1 = I_2$. The reason to study this case is twofold: on the one hand this resonance is generic, in the sense that it is not trivially related to a normally hyperbolic invariant manifold such as the resonance $I_1 = 0$; on the other hand it is the resonance which we studied in the papers [19],[20]. In figure 5 we report the computation of the FLI for values of ϵ ranging from 0.04 up to 0.4. The coordinates of the pictures are $x = I_2 - I_1/2$, $y = I_1 + 2I_2$, so that the resonance is almost vertical. In all the pictures we appreciate the presence of an hyperbolic structure which plays the role of the normally hyperbolic invariant manifold Λ. We will refer to this structure as to the hyperbolic set of the resonance. Around this hyperbolic set we observe also the presence of the petals structures (which will be explained in section 4) related to the dominant resonances. As for the previous case, at different values of ϵ the dominant petals structures which characterize the topology of the stable manifold are different, according to the local dominant resonances. In fact, for $\epsilon = 0.04$ (top left panel of figure 5) we detect only one petals structure centered around a resonance which cross the hyperbolic invariant set in the middle of the figure. For $\epsilon = 0.1$ (top right panel of figure 5) in the same region of the phase–space we observe also the petals of structures which do not belong to the central one, but are centered around resonances which are outside the upper and the lower sides of the picture. For $\epsilon = 0.22$ (bottom left panel of figure 5) the upper and lower structures have become dominant with respect to the central one, which is no more evident in this picture. For $\epsilon = 0.4$ the upper and lower structures are overlapping in correspondence of the central resonance. It is clear that these transitions in the topology of the stable manifold are related to the local dominant resonances, which are different at different values of ϵ. We also observe that these transitions in the topology of the stable manifold are related to the changes of the slopes characterizing the dependence of the diffusion coefficient on ϵ, in a log-log scale (see figure 6 of [20]). In fact, $\epsilon = 0.04$ is in the

interval characterized by $D(\epsilon) \sim \epsilon^{m3}$, with $m3 \sim 13.3$; $\epsilon = 0.1$ is in the transition between the law $D(\epsilon) \sim \epsilon^{m3}$ and the law $D(\epsilon) \sim \epsilon^{m2}$, with $m2 \sim 8.5$; $\epsilon = 0.22$ is in the interval characterized by $D(\epsilon) \sim \epsilon^{m2}$ and $\epsilon = 0.4$ is in the interval characterized by $D(\epsilon) \sim \epsilon^{m1}$, with $m1 = 4.2$. Therefore the intervals characterized by a given slope correspond approximately to the different resonances dominating the topology of the stable manifold.

4 Topology of the asymptotic manifolds in the case of two weakly interacting resonances

We found in the previous section a topology very different from the one detected for the a priori unstable cases. We find that stable and unstable manifolds in quasi–integrable systems are characterized by the presence at any scale of peculiar structures, made by many petals. We will call these structures flower–like. We explain them as due to the interaction among the resonances. In this section we show that a model with two weakly interacting resonances of the same amplitude can explain the presence of the flower–like structures. Precisely, we consider the Hamiltonian system with Hamilton function:

$$H(I_1, I_2, \varphi_1, \varphi_2) = \frac{I_1^2}{2} + \frac{I_2^2}{2} - a_1 \cos(\varphi_1) - a_2 \cos(\varphi_2) - \epsilon \cos(\varphi_1)\cos(\varphi_2) \ . \tag{11}$$

When a_1, a_2 are of order 1 this is an a priori unstable system, but instability is present in both degrees of freedom. The interaction among the two resonances is represented by the perturbation.

Remark. The normal form of a generic n degree of freedom Hamiltonian system $H(I, \varphi) = h(I) + \eta f(I, \varphi)$ near a double resonance takes the form, in suitable scaled action-angle variables J, ψ [9],

$$\mathcal{H}(J, \psi) = k(J) + g(\psi_1, \psi_2) + \sqrt{\eta} u(J, \psi_1, \psi_2; \eta) + \exp - \left(\frac{\eta_0}{\eta}\right)^{\frac{1}{2n}} v(J, \psi; \eta) \ . \tag{12}$$

In the frequent case of double resonances characterized by two dominating harmonics the function g can be written in the form:

$$g = g_1(\psi_1) + g_2(\psi_2) + \epsilon g_{12}(\psi_1, \psi_2) \quad ,$$

so that the dominant part of (12) is very similar to (11).

Returning to Hamiltonian (11), we remark that it has the normally hyperbolic invariant manifold:

$$\Lambda = \{(I_1, I_2, \varphi_2, \varphi_2) : \quad \varphi_1 = \pi \quad , \quad I_1 = 0\} \quad ,$$

(as well as other ones) and we want to describe its asymptotic manifolds. In figure 6 on the left we can appreciate that the asymptotic manifolds have a peculiar flower–like structure. We now approximate the equation for the variable φ_1 as follows:

$$\ddot{\varphi}_1 = -\sin(\varphi_1)\Big(a_1 + \epsilon\cos(\varphi_2^0(t))\Big) + \mathcal{O}(\epsilon^2)$$

where $\varphi_2^0(t)$ is the order–0 solution for φ_2, i.e. $\ddot{\varphi}_2^0 = -a_2\sin(\varphi_2^0)$. Therefore, we study the approximate equation:

$$\ddot{\varphi}_1 = -\sin(\varphi_1)\Big(a_1 + \epsilon\cos(\varphi_2^0(t))\Big) \tag{13}$$

and describe the topology of the asymptotic manifolds of the fixed point $(\varphi_1, \dot{\varphi}_1) = (\pi, 0)$. In figure 6 on the right we can appreciate that the asymptotic manifolds of Λ for the approximated systems are accurately reproduced, except for the region very close to the resonance $I_2 = 0$, where the approximation (13) is not accurate. We now describe the asymptotic manifolds of equation (13). For any initial condition $\varphi_2^0(0) = \pi, \dot{\varphi}_2(0) = I_2(0)$ the function $\varphi_2^0(t)$ is periodic with some period $T(I_2(0))$. For any fixed $I_2(0)$, we consider the Poincaré section ϕ^T at time T of the Hamiltonian system:

$$H = \frac{I_1^2}{2} - a_1\cos(\varphi_1) - \epsilon\cos(\varphi_1)\cos(\varphi_2^0(t)) \quad . \tag{14}$$

The stable and unstable manifolds of the fixed point $x = (\varphi_1, I_1) = (\pi, 0)$ for the map ϕ^T are characterized by the well known structure of the homoclinic tangle of 2–dimensional maps. We consider $W_s(x)$ and its first four intersections with the axis $\varphi_1 = \pi$, which are marked with stars in figure 7. By changing $I_2(0)$, the intersection points of the unstable manifold with the axis $\varphi_1 = \pi$ change as well, describing arcs on the section S. When a lobe of the homoclinic tangle becomes tangent to the axis $\varphi_1 = \pi$, two arcs of intersection points on the section S are joint together, and they constitute the upper part of a petal of the flower–like structure. By moving $I_2(0)$ towards zero, the value of I_2 of the intersection points goes to zero as well, because for $I_2(0) = 0$ the function $\varphi_2^0(t)$ is constant with respect to time, and therefore the system is integrable and the unstable manifold does not have lobes. Therefore, the generation of a petal of the flower–like structure is the following: starting from the exact resonance we find the basis of the petal; increasing $I_2(0)$, i.e. going away from the resonance, a lobe intersects the section producing the two arcs of the petal, which are joint together for the value of $I_2(0)$ at which that lobe is tangent to the section.

It is important to remark that each petal is the intersection of the stable/unstable manifold of Λ, i.e. of the single resonance $\dot{\varphi}_1 = 0$, with

the section S, and not the intersection of S with the stable/unstable manifold of a double resonance. Therefore, these structures are centered on the double resonances, but are part of the asymptotic manifolds of the single resonances.

In a fully interacting system, like the map ϕ, we can observe many of these flower–like structures centered around the crossing of resonances, as it is the case of figure 8.

5 Measure of the exponential splitting of the homoclinic tangle

In the aim of finding a connection between the invariant manifold Λ and the diffusion along the resonance $I_1 = 0$ we computed the unstable manifold of Λ for $\epsilon \neq 0$, $c = 2.1$, and we choose an interval of I_2 far from the main crossings of Λ with the other resonances. For example, figure 9 (left panel) shows the phase portrait of the plane (φ_1, I_1) for $\epsilon = -10^{-5}$ of a set of 40 orbits regularly spaced in $I_1(0) \in (-0.008, 0.008)$. The other initial conditions are $\varphi_1(0) = \pi$, $\varphi_2(0) = 0$, $I_2(0) = 0.397499949$. The points of the 40 orbits satisfying $|\varphi_2| \leq 10^{-3}$ are plotted. We can observe the typical phase portrait of single resonances, characterized by the presence of invariant KAM tori, a libration island and a chaotic region generated by the hyperbolic point at the origin and surrounding the libration island.

In the regime of validity of the Nekhoroshev theorem we expect that a normal form like (6) is valid. For comparison, in figure 9 (right panel) we report also the phase portrait of the main part the normal form (6), i.e. the phase portrait of the map generated by $I' \cdot \varphi + {I'_1}^2/2 + {I'_2}^2/2 + \epsilon u_0(\varphi_1)$. The most evident difference among the two phase portraits is the chaotic zone which appears around the hyperbolic point of the complete map (figure 9 left), which is due to the remainder $\mathcal{R}$, i.e. the only part of the normal form which depends on φ_2. In fact, in the single resonance domain related to the resonance $I_1 = 0$, if one neglects the exponentially small remainder one remains with a generating function of a two dimensional generalized standard map. It is known (see [14],[15]) that in the limit of small ϵ the thickness of the chaotic region related to the hyperbolic point of the resonance decreases asymptotically exponentially with $1/\sqrt{\epsilon}$. In the present case, with the actual value of ϵ, the phase portrait reported in figure 9 (right panel) shows that this chaotic zone is indeed so small that we do not detect it in the figure. If we consider the complete map the chaotic region related to the hyperbolic fixed point of the resonance can be larger, because now the normal form is in general corrected by the additional exponentially small remainder depending also on I_2, φ_2. With the actual value of ϵ it is clear that the chaotic zone in figure 9

ϵ	N	$\bar{t}$	$\Delta\varphi_1$
-10^{-9}	10^3	$9\,10^6$	10^{-29}
-10^{-8}	10^3	$3\,10^6$	10^{-24}
-10^{-7}	$2\,10^3$	$7\,10^5$	10^{-18}
-10^{-6}	$5\,10^4$	10^5	10^{-5}
-10^{-5}	$5\,10^4$	$8\,10^3$	10^{-3}

Table 1: Parameters for the detection of the unstable manifold of the hyperbolic point $(\varphi_1, I_1) = (0, 0)$

(left panel) is due to the remainder $\mathcal{R}$. By changing the value of ϵ, we find that the chaotic zone decreases approximately exponentially with $1/\epsilon^{1/3}$. Though we are not aware of the existence of an asymptotic formula describing the splitting of the stable/unstable manifolds in this specific case (for the computation of the splitting in other models see, for example, [16]), this behavior is due to the remainder $\mathcal{R}$ of the Nekhoroshev normal form (6) for that resonance, which is therefore exponentially small as well. Now we describe how we solved the problem of the numerical detection of this exponentially small quantity. We expect that in the regime of validity of the Nekhoroshev theorem the size of the chaotic zone at a distance d from the hyperbolic point depends on ϵ approximately like:

$$L_d(\epsilon) = f(d)\, \exp\Big(- \Big(\frac{\epsilon^*}{\epsilon}\Big)^{\alpha} \Big) \quad , \tag{15}$$

where the function f and the constants ϵ^*, α are unknown and must be determined by a numerical fit.

We have detected the unstable manifold related to $(\varphi_1, I_1) = (0, 0)$ using the classical method of propagating a set of N initial conditions taken in the neighborhood of size $\Delta\varphi_1$ of the hyperbolic point. Figure 10 shows the points of the N orbits intersecting the section $|\varphi_2| \leq 10^{-3}$ for different values of ϵ. The number of orbits N, the integration time $\bar{t}$ and the interval $\Delta\varphi_1$ are suitably chosen for each value of ϵ and the numerical values of such quantities are provided in Table 1. The unstable manifold is characterized by typical lobes.

The zooms out around the origin, from the panel at top left to the panel at bottom right, illustrate visually the strong decrease of the size of the lobes of the unstable manifold by changing the perturbing parameter. To measure the size of the chaotic zone we compute the amplitude of the lobes detected in figure 10, i.e. we measure the function $L_d(\epsilon)$ as the distance between the maximum and the mini-

mum of a lobe located at a distance d from the hyperbolic point. In order to obtain a numerical evidence of the exponential character of $S(\epsilon) = L_d(\epsilon)/f(d)$ we cannot simply fix d and measure $L_d(\epsilon)$ by changing ϵ, because, for fixed d, we would be able to measure effectively the amplitude of the lobes only through a small interval in ϵ. In fact, due to the strong decreasing of the amplitudes with ϵ, from figure 10 it appears clearly that the lobes are detected up to a maximal distance d_{max} from the hyperbolic point which reduces drastically with ϵ. In order to obtain a numerical measure of $S(\epsilon) = L_d(\epsilon)/f(d)$ through many orders of magnitude in ϵ we need therefore a numerical fit for $f(d)$, so that, for any ϵ, we can suitably choose the distance d.

We fit the function $f(d)$ using the numerical computation of $L_\epsilon(d)$ for different values of ϵ (figure 11). Each data set is well fitted by a power law: d^{m_ϵ}, and the set of the slopes m_ϵ has mean value $\bar{m} = -1.25$ and standard deviation $\sigma = 0.06$. We will consider the function $d^{\bar{m}}$ as a good fit of $f(d)$ in eq. (15).

Figure 12 shows the logarithm of $1/S$ as a function of the logarithm of $1/\epsilon$. The exponential dependence of S on ϵ appears clearly. We have repeated the experiment by filling the chaotic region as in figure 9 and measuring its size at a suited distance d from the hyperbolic fixed point. The distance dependence is normalized with the function $d^{\bar{m}}$ previously computed. Figure 12 shows that the size of the separatrix splitting can be obtained both by directly measuring the lobes or the size of the corresponding chaotic region.

Thanks to the fact that the measure spans 5 orders of magnitude in ϵ, we could fit the parameter α by taking the double logarithm of $S(\epsilon)$ (see fig. 13). The numerical computation confirms the validity of eq. (15), with $\alpha = 0.33 \sim 1/3$.

6 Detection of the topological mechanism for Arnold diffusion

In the previous sections we have shown that the topology of the stable/unstable manifolds of the invariant manifold Λ is correlated to the diffusion properties along Λ: in section 3 we have shown that, by changing ϵ, the topology has transitions which approximately correspond to the changes of the slopes of the diffusion coefficient versus ϵ in the log/log representation; in section 5 we have shown that the amplitude of the lobes of the homoclinic tangle is decreasing exponentially with $1/\epsilon^{1/3}$, and we attributed this scaling to the exponentially decrease of the remainder of the resonant normal form, as in the case of the

validity of the Nekhoroshev theorem. These facts provide indications of the correlations among the exponentially small remainder of the resonant normal forms around Λ, the topology of the stable/unstable manifolds of Λ and the diffusion coefficient along Λ. However, they do not not allow one to understand how the stable/unstable manifolds are directly related to the diffusion along Λ. In this section we will explain this mechanism by showing that the unstable manifolds of the points $x \in \Lambda$ are unrolled along the I_2 direction, with possible many large oscillations, but with an average systematic drift. In fact, the oscillations of the unstable manifolds along the I_2 direction are similar to the large oscillations that the single orbits do during their Arnold diffusion along Λ, and also in that case we needed to perform averages and filters on the data to show the existence of a very slow diffusion. The existence of a systematic drift of the unstable manifold in the I_2 direction shows how the diffusion along Λ takes place: given a generic point x in the invariant manifold, the dynamics maps the points in a neighborhood U of x along the unstable manifold of x, and because of the spread of this unstable manifold, the set U spreads in the phase space and some of its points return near the invariant manifold 'far away' from the orbit of x. This is the mechanism that we detect and that is behind the Arnold diffusion phenomena shown in the papers [18], [19],[20].

As for the a priori unstable case of [2], we do not directly detect transitions of orbits from stable to unstable manifolds, but this is likely due to the fact that the probability of finding an orbit which passes near selected number of heteroclinic points is very small. The existence of heteroclinic transverse intersections remains a possible way to prove the spread of the asymptotic manifolds in certain situations.

We now describe our results on the computation of the parametrization of the unstable manifold W_u of the invariant manifold Λ for quite a long arc–length s, for values of ϵ lower than the critical value for the transition of the system to the Chirikov regime. Using the FLI charts we have found that the transition between the Nekhoroshev and the Chirikov regime occurs in the interval $3\,10^{-4} < \epsilon < 4\,10^{-4}$. This threshold is lower than the value $\epsilon_c \simeq 0.002$ (see section 1) which bounds diffusion on Λ, i.e. of the limit value for the validity of our numerical method.

In this section our numerical experiments concern the two values $\epsilon = 9\ 10^{-5}$ and $3\ 10^{-4}$, so that we first check if the invariant manifold Λ is normally hyperbolic for these values of ϵ. We do it numerically, following the technique that we introduced in paper [2]. Precisely, we choose the tangent vectors norm: $\|(\xi_{\varphi_1}, \xi_{\varphi_2}, \xi_{I_1}, \xi_{I_2})\|^2 = |\xi_{\varphi_1}|^2 + |\xi_{\varphi_2}|^2 + |\xi_{I_1}|^2 + |\xi_{I_2}|^2$ and we check if the map ϕ^N is hyperbolic for some integer N. For each point x of a grid of initial conditions with $I_2 \in [0, 2]$, $I_1 = 0$, $\varphi_1 = \pi$, $\varphi_2 = 0$ we first computed the Lyapunov

exponents of the map ϕ (up to a $N = 10^4$ iterations) for initial tangent vectors in the tangent space $T_x\Lambda^{ort}$ orthogonal to $T_x\Lambda$, i.e. for vectors of the form $\xi = (\xi_{\varphi_1}, 0, \xi_{I_1}, 0)$. For $\epsilon = 9\ 10^{-5}$ we measured a positive Lyapunov exponent bigger than $5\ 10^{-3}$ for all the points of the grid, and of course a negative Lyapunov exponent smaller than $-5\ 10^{-3}$, while for $\epsilon = 3\ 10^{-4}$ we measured a positive Lyapunov exponent bigger than $8\ 10^{-3}$ for all the points of the grid (the negative Lyapunov exponent is smaller than $-8\ 10^{-3}$). This is an indication of the hyperbolic splitting of the space $T_x\Lambda^{ort}$ as a direct sum of a stable space $E^s(x)$ and an unstable space $E^u(x)$. The numerical algorithm for the computation of the Lyapunov characteristic exponents provides also an estimate of the constants $\lambda_1 = \mu_1$ and $\lambda_3 = \mu_3$ which are related to an iterate ϕ^N of ϕ (see paper [2] for the definitions). In fact, if N is sufficiently large, the quantities $1/\exp(FLI(N))$ and $\exp(FLI(N))$ converge exponentially to λ_1 and λ_3 for almost any initial tangent vector $\xi \in T_x\Lambda^{ort}$ ($FLI(N)$ denotes the Fast Lyapunov indicator computed up to N iterations of the map ϕ). It remains to estimate the constants λ_2, μ_2 (see paper [2] for the definitions) for the map ϕ^N in the point x. Because in this case the growth of initial tangent vectors $\xi = (0, \xi_{\varphi_2}, 0, \xi_{I_2}) \in T_x\Lambda$ is not expected to be always exponential, we did not computed the Lyapunov characteristic exponents, but we computed numerically the two dimensional matrix representing the restriction of $D\phi^N(x)$ to the space $T_x\Lambda$. This can be done by computing the evolution of a bases of two independent vectors of $T_x\Lambda$. Once the matrix $D\phi^N(x)$ was obtained, we computed directly the quantities:

$$\lambda_2 \leq \inf_{\xi \in T_x\Lambda \setminus 0} \frac{\|D\phi^N(x)\xi\|}{\|\xi\|} \leq \sup_{\xi \in T_x\Lambda \setminus 0} \frac{\|D\phi^N(x)\xi\|}{\|\xi\|} \leq \mu_2 \quad .$$

Figure 14 shows the numerical computation of $\log \lambda_2/N$ and $\log \mu_2/N$ for $N = 10000$ and respectively $\epsilon = 9\ 10^{-5}$ (left panel) and $\epsilon = 3\ 10^{-4}$ (right panel). From the comparison of the four computed quantities $\log \lambda_1$, $\log \lambda_2$, $\log \mu_2$, $\log \lambda_3$ we infer that the invariant manifold Λ is normally hyperbolic for both $\epsilon = 9\ 10^{-5}$ and $\epsilon = 3\ 10^{-4}$.

After having checked that Λ is normally hyperbolic, we computed the parametrization:

$$s \longmapsto (\varphi_1(s), I_1(s), \varphi_2(s), I_2(s))$$

of the unstable manifold $W_u(x)$ of a point $x = (\varphi_1, I_1, \varphi_2, I_2) = (\pi, 0, 0, 0.324)$, with respect to its arc–length. The method used for this computation is described in paper [2], section 2, and we refer to that paper for the technical details. Here, we report the result of the computations.

For $\epsilon = 9\ 10^{-5}$, the point x belongs to an invariant torus of $\phi_{|\Lambda}$ (see figure 15, left panel). Figure 15 (right panel) shows the result

of the computation of $I_1(s)$ versus the arc–lenght s parametrizing the unstable manifold $W_u(x)$. To discuss the relation among the unstable manifold $W_u(x)$ and the diffusion properties along Λ the most interesting quantity is the dependence of $I_2(s)$ on the arc–length s, which is reported in figure 16, left panel. From that figure it appears that $I_2(s)$ undergoes many large fluctuations, but it is very difficult to appreciate the presence of an eventual systematic drift, which would be related to the diffusion along Λ. In order to reveal an eventual drift of $I_2(s)$ we need to filter with respect to φ_1 the large variations of I_2 by selecting the points of $W_u(x)$ characterized by $-0.5 < \varphi_1 < 0.5$ and $I_1 > 0$. These selected points are reported in figure 16, right panel, and clearly reveal a drift of $I_2(s)$ as a function of the arc–lenght s. Reducing the tolerance on φ_1 reduces the number of selected points but the drift of I_2 is still present.

The dependence of I_2 on φ_1 appears clearly on the 3-dimensional representation of the manifold (figure 17, left panel). Also with this representation we can appreciate the spread of the unstable manifold by selecting the points in the interval $-0.5 < \varphi_1 < 0.5$, with $I_1 > 0$, which are reported in figure 17, right panel. We can therefore infer for this value of $\epsilon \neq 0$ that the manifold is unrolled along the I_2 direction, thus supporting diffusion in the neighborhood of Λ. At our knowledge this is the first computation of stable/unstable manifolds of a quasi–integrable system which shows the topological mechanism which produces diffusion of orbits, in the range of the perturbing parameters satisfying the hypothesis of the Nekhoroshev theorem.

In order to remark a systematic spread of the manifolds in the I_2 direction we computed also the quadratic average of the quantity $(I_2(s) - I_2(0))$ with respect to many close initial points. As in the a priori unstable case we use the fact that the arc-lenght and time are approximately related through: $s(t) \sim s(0)\exp(\lambda t)$, where λ is the Lyapunov exponent, which we computed over $t = 10^9$ iterations and averaged over $N = 20$ orbits with initial conditions $-10^{-5} < I_1 < 10^{-5}$, $\varphi_1 = \pi$, $0.3 < I_2 < 0.4$, $\varphi_2 = 0$. In figure 18 (dashed line) we represent the quantity:

$$G(t) = \frac{1}{N} \sum_{j=1,|\varphi_1^j(s(t))|<0.1}^{N} \left(I_2^j(s(t)) - I_2^j(s(0)) \right)^2 \qquad (16)$$

versus t for $\epsilon = 3\,10^{-4}$ ($N = 40$, the initial conditions are $I_1 = 0$, $\varphi_1 = \pi$, $0.3 < I_2 < 0.4$, $\varphi_2 = 0$).

It is clear that we measure a positive average quadratic spread of the manifold, while we are not able to fit this quantity to estimate the linear growth of $G(t)$, as we did in the a priori unstable case, although ϵ is very close to the threshold from the Nekhoroshev to the Chirikov behavior. We have therefore compared this result to the

classical method of diffusion of orbits [18],[19] in the phase space. To this purpose we computed the average evolution of the mean squared distance from the initial conditions for the same set of initial conditions, same ϵ and same filter on the angles than figure 18 (dashed line). The result is reported in figure 18 (continuous line), and it appears that in order to obtain a systematic linear growth of $G(t)$ the total time must be about 5 times larger than the one which corresponds to the manifold computation, and because of the exponential relation among time and arch–length this is out of the present computational possibilities. However we remark that the quantity $G(t)$ computed on the unstable manifold is very similar to that obtained with the diffusion of particles.

Although we do not compute a 'geometric' diffusion coefficient for the stable case it is interesting to compare the spread of the manifold of one orbit for two different values of ϵ. In this aim we studied the orbit of figure 17 for $\epsilon = 2\,10^{-4}$ (figure 19).

We appreciate the unrolling of the manifold in the I_2 direction already on the global representation of the orbit (figure 19, left panel). Comparing the zoomed pictures represented in the right panels of figures 17 and 19 we see that the square of the manifold spread $(I_2(s) - I_2(0))^2$ for $\epsilon = 2\,10^{-4}$ is about 5 order of magnitudes larger than for $\epsilon = 9\,10^{-5}$. This is exactly the ratio among the corresponding diffusion coefficients (see figure 3). This is a confirmation that the Arnold diffusion that we measured in [18],[19],[20] is supported by the unrolling of the manifolds along the resonance.

7 Appendix: the Fast Lyapunov Indicator

A precise numerical detection of the dynamical character of an orbit is possible with the Fast Lyapunov Indicator whose definition is related to the Lyapunov exponent theory. In the numerical computations of the Lyapunov Characteristics Indicator (LCI hereafter) the attention is focused on the length of time necessary to get a reliable value of its limit, while very little importance is given to the first part of the computation. Actually, this part is usually considered as a kind of transitory regime depending, among other factors, on the choice of an initial vector of the tangent manifold.

In 1997, Froeschlé et al. [11] have remarked that the intermediate value of the largest LCI (which was called fast Lyapunov Indicator: FLI hereafter), taken at equal times for chaotic, even weakly chaotic, and ordered motions, allows one to distinguish between them. It turns out that the FLI allows also to distinguish among ordered motions of different origins, like resonant and non resonant motions [17]. This is not possible with the LCI, which tends to zero when t goes to infinity

in both cases.

Given a map ϕ from $\mathbb{R}^n$ to $\mathbb{R}^n$, an initial condition $x(0) \in \mathbb{R}^n$, and an initial vector $v(0) \in \mathbb{R}^n$ of norm one, let us define the FLI function $FLI(x(0), v(0), T)$, $T > 0$, as:

$$FLI(x(0), v(0), T) = \sup_{0<t\leq T} \log ||v(t)|| \,, \tag{17}$$

where $v(t)$ is given by the system:

$$\left\{ \begin{array}{lcl} x(t+1) & = & \phi(x(t)) \\ v(t+1) & = & \frac{\partial \phi}{\partial x}(x(t))\, v(t) \,. \end{array} \right. \tag{18}$$

The definition trivially extends to continuous flows. In the specific case of quasi-integrable Hamiltonian systems:

$$H_\epsilon(I, \varphi) = h(I) + \epsilon f(I, \varphi) \quad , \tag{19}$$

for any initial condition $(I(0), \varphi(0))$ and any initial tangent vector $(v_I(0), v_\varphi(0))$, the FLI at time t is:

$$\log \|(v_I(t), v_\varphi(t))\| \quad . \tag{20}$$

In order to kill non significant fluctuations of (20), in formula (17) we have considered the supremum of the logarithm of the norm of the tangent vector. A running average could also have been used. Actually, as far as the mathematical development is concerned, we drop these averaging procedures, which however are useful in numerical computations. For $\epsilon = 0$ it is evidently:

$$v_I^0(t) = v_I(0) \quad , \quad v_\varphi^0(t) = v_\varphi(0) + \frac{\partial^2 h}{\partial^2 I}(I(0)) v_I(0) t \quad .$$

If ϵ is small we can estimate the evolution of $||v||$ with Hamiltonian perturbation theory. Following [17], if the initial condition is on a KAM torus then the norm $||v^\epsilon(t)||$ satisfies:

$$||v^\epsilon(t)|| = \left\| \frac{\partial^2 h}{\partial^2 I}(I(0)) v_I(0) \right\| t + \mathcal{O}(\epsilon^\alpha t) + \mathcal{O}(1) \quad , \tag{21}$$

with some $\alpha > 0$. As a consequence, the FLI has approximately the value of the unperturbed case on all KAM tori. Instead if the initial condition is on a regular resonant motion then it is [17]:

$$||v^\epsilon(t)|| = \|C_\Lambda \Pi_{\Lambda^{ort}} v_I(0)\|\, t + \mathcal{O}(\epsilon^\beta t) + t\mathcal{O}(\rho^2) + \mathcal{O}(\sqrt{\epsilon} t) + \mathcal{O}(\frac{1}{\sqrt{\epsilon}}) \tag{22}$$

with some $\beta > 0$, Λ^{ort} being the linear space orthogonal to an integer lattice Λ (the integer lattice $\Lambda \subseteq Z^n$ defines the resonance, see [17] for

details), C_Λ is a linear operator depending on the resonant lattice Λ and on the initial action $I(0)$, $\Pi_{\Lambda^{ort}}$ denotes the projection over the lattice Λ^{ort}.

It is important to remark that the FLI on regular resonant motions is different at order $\mathcal{O}(1)$ from the unperturbed case on regular resonant motions. In fact, the linear operator $C_\Lambda \Pi_{\Lambda^{ort}}$ is different from the Hessian matrix of h at order $\mathcal{O}(1)$, i.e. $C_\Lambda \Pi_{\Lambda^{ort}}$ does not approach $\frac{\partial^2 h}{\partial I^2}$ as ϵ approaches to zero. In this way, we detect the presence of the resonances because the value of the FLI is different from the uniform value assumed on the KAM tori. Finally, for initial conditions on chaotic resonant motions the FLI is higher (since the tangent vectors growth exponentially with time) than the value characterizing KAM tori. As a consequence the resonance structure of the phase space can be detected computing the FLI with the same $v(0)$ and the same time interval t on a grid of regularly spaced initial conditions. The representation of the set of resonances of a quasi–integrable Hamiltonian system can be found in [13].

We have found in [2] a new application of the FLI method that allows a sharp detection of the intersection of the stable and unstable manifolds of the normally hyperbolic invariant manifolds with any two dimensional section of the phase–space. The principle is the following. We sample the two dimensional section of the phase space with a grid of points. Then, for any point of the grid we compute the FLI up to a time T. The points of the grid which will have the highest values of the FLI are those points whose orbits approach an hyperbolic invariant manifold within the time T, because the growth of tangent vectors is bigger near the hyperbolic manifolds. Therefore, a short–time computation of the FLI allows to detect a neighborhood of a finite piece of the stable manifold (for the unstable manifold one repeats the computation using the inverse map).

Acknowledgments. We wish to thank C. Efthymiopoulos for interesting discussions through all these years about Arnold diffusion.

M. Guzzo has been supported by the project CPDA063945/06 of the University of Padova.

References

References

[1] Arnold V.I.: Instability of dynamical systems with several degrees of freedom. Sov. Math. Dokl., 6, 581–585, 1964.

[2] Lega E., Guzzo M. and Froeschlé C.: A numerical study of the topology of hyperbolic manifolds supporting diffusion in a priori unstable systems. Preprint, 2007.

[3] Hirsch M.W., Pugh C.C. and Shub M.: Invariant Manifolds. Lecture Notes in Mathematics, Vol. 583. Springer-Verlag, Berlin-New York, 1977.

[4] Chierchia L. and Gallavotti G.: Drift and diffusion in phase space. Ann. Inst. H.Poincaré, Vol. 60, 1–144, 1994.

[5] Chierchia L. and Valdinoci E.: A note on the construction of Hamiltonian trajectories along heteroclinic chains. Forum Math., Vol. 12, 247–255, 2000.

[6] Delshams A., de la Llave R. and Seara T. M.: A geometric mechanism for diffusion in Hamiltonian systems overcoming the large gap problem: heuristics and rigorous verification on a model. Mem. Amer. Math. Soc. 179, no. 844 (2006).

[7] Chirikov B.V.: An universal instability of many dimensional oscillator system. Phys. Reports, 52:265, (1979).

[8] Hasselblatt B. and Pesin Y.: Partially hyperbolic dynamical systems. Handbook of dynamical systems. Vol. 1B, 1–55, Elsevier B. V., Amsterdam, 2006.

[9] Benettin, G. and Gallavotti G.: Stability of motions near resonances in quasi–integrable Hamiltonian systems. J. Stat. Phys., vol. 44, 293–338, 1986.

[10] Guzzo M.: A direct proof of the Nekhoroshev theorem for nearly integrable symplectic maps. Annales Henry Poincaré, vol. 5, n. 6, 1013-1039, 2004.

[11] Froeschlé C., Lega E. and Gonczi R.: Fast lyapunov indicators. application to asteroidal motion. Celest. Mech. and Dynam. Astron., Vol. 67, 41–62, 1997.

[12] Froeschlé C., Gonczi R. and Lega E.: The fast lyapunov indicator: a simple tool to detect weak chaos. application to the structure of the main asteroidal belt. *Planetary and space science*, Vol. 45, 881–886, 1997.

[13] Froeschlé C., Guzzo M. and Lega E.: "Graphical Evolution of the Arnold Web: From Order to Chaos". Science, Volume 289, n. 5487, 2000.

[14] Gelfreich V. G., Lazutkin, V. F. and Tabanov, M. B.: "Exponentially small splittings in Hamiltonian systems." Chaos 1, no. 2, 137–142, 1991.

[15] Gelfreich V. G.: "A proof of the exponentially small transversality of the separatrices for the standard map." Comm. Math. Phys. 201, no. 1, 155–216, 1999.

[16] Morbidelli A. and Giorgilli A.: On the role of high order resonances in normal forms and in separatrix splitting. Physica D, vol. 102, 195–207, 1997.

[17] Guzzo M., Lega E. and Froeschlé C.: On the numerical detection of the effective stability of chaotic motions in quasi-integrable systems. Physica D, Volume 163, Issues 1-2, 1-25, 2002.

[18] Lega E., Guzzo M. and Froeschlé C.: "Detection of Arnold diffusion in Hamiltonian systems". Physica D, vol. 182, p. 179–187, 2003.

[19] Guzzo M., Lega E. and Froeschlé C.: "First Numerical Evidence of Arnold diffusion in quasi–integrable systems". DCDS B, vol. 5, n. 3, 2005.

[20] Froeschlé C., Guzzo M. and Lega E.: "Local and global diffusion along resonant lines in discrete quasi–integrable dynamical systems", Celestial Mechanics and Dynamical Astronomy, vol. 92, n. 1-3, 243-255, 2005.

[21] Guzzo M., Lega E. and Froeschlé C.: Diffusion and stability in perturbed non-convex integrable systems. Nonlinearity, **19**, pp 1049–1067, (2006).

[22] Kuksin, S. B.: On the inclusion of an almost integrable analytic symplectomorphism into a Hamiltonian flow. Russian journal of Mathematical Physics, **1**, 2, 191–207 (1993).

[23] Kuksin, S. and Pöschel, J.: On the inclusion of analytic symplectic maps in analytic Hamiltonian flows and its applications. Seminar on Dynamical Systems (St. Petersburg, 1991), 96–116, Progr. Nonlinear Differential Equations Appl., 12, Birkhäuser, Basel (1994).

[24] Mather J.N.: Arnold diffusion, I: announcement of results. Contemporary Mathematics and its Applications, Fundamental Directions April–May 2003 (Russian transl.), original to appear in J. Math. Sci.

[25] Treschev D.: Trajectories in a neighbourhood of asymptotic surfaces of a priori unstable Hamiltonian systems. Nonlinearity 15 2033-2052, 2002.

[26] Treschev D.: Evolution of slow variables in a priori unstable Hamiltonian systems. Nonlinearity 17 1803-1841, 2004.

[27] Simo C.: On the analytical and numercial approximation of invariant manifolds, in Modern Methods in Celestial Mechanics, D. Benest, Cl. Froeschlé eds, Editions Frontières, 285-329, 1989.

[28] Krauskopf B., Osinga H.M., Doedel E.J., Henderson Enheimer J., Vladimirsky A., Dellnitz M., Junge O.: A survey of methods for computing (un)stable manifolds of vector fields. Int. J. Bif. and Chaos, **15**, 763-791, 2005.

[29] Broer H.W., Osinga H.M. and Vegter G.: Algorithms for computing normally hyperbolic invariant manifolds. ZAMP **48**, 480-524, 1997.

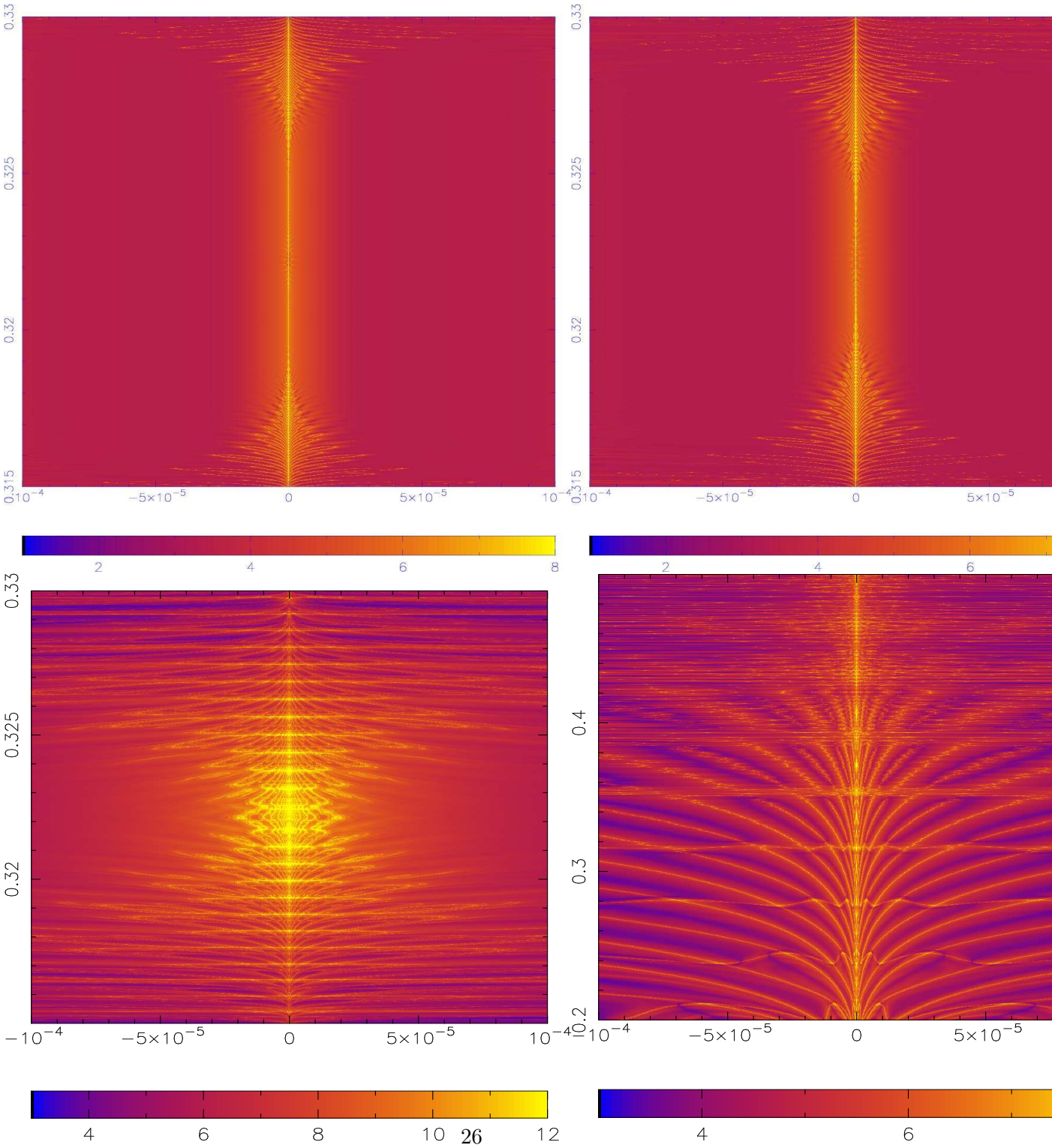

Figure 4: Computation of the FLI on the surface S for values of $\epsilon = 6\ 10^{-6}, 10^{-5}$ (on the top) and $\epsilon = 4\ 10^{-5}, 4\ 10^{-4}$ (on the bottom). The coordinates of the pictures are $x = I_1$, $y = I_2$.

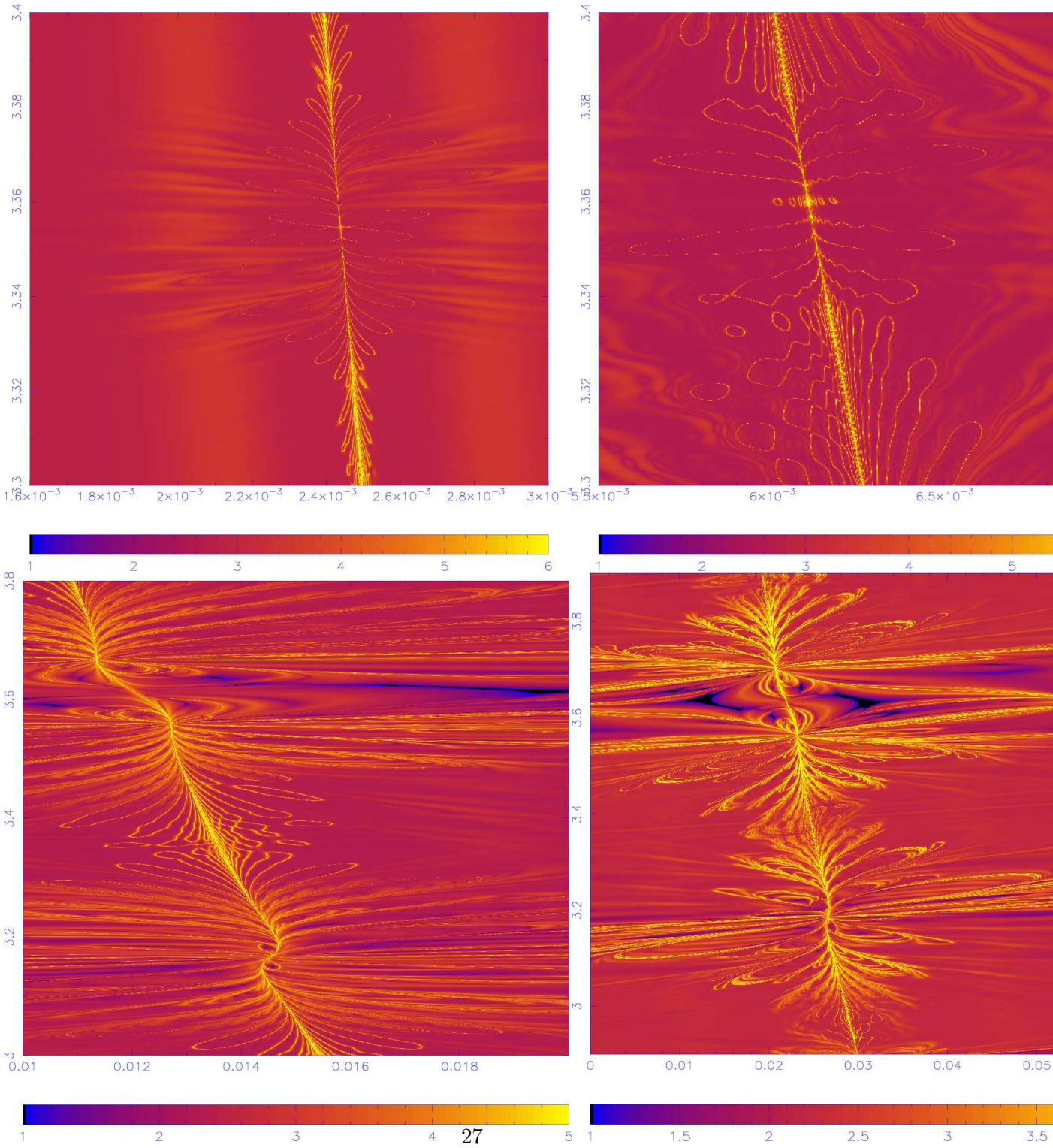

Figure 5: Computation of the FLI for values of $\epsilon = 0.04, 0.1$ (on the top) and $\epsilon = 0.22, 0.4$ (on the bottom). The coordinates of the pictures are $x = I_2 - I_1/2$, $y = I_1 + 2I_2$, so that the resonance is almost vertical.

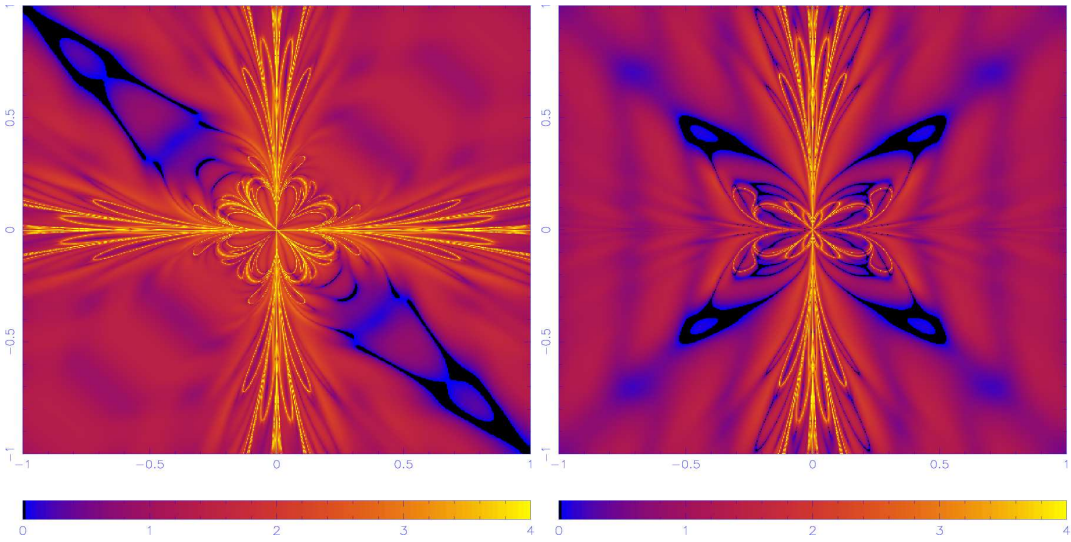

Figure 6: **On the left:** asymptotic manifolds of the hyperbolic invariant manifolds of Hamiltonian systems (11), for $a = 1$ and $\epsilon = 0.01$. **On the right:** asymptotic manifolds of the hyperbolic invariant manifolds of the approximated system (13), for $a = 1$ and $\epsilon = 0.01$.

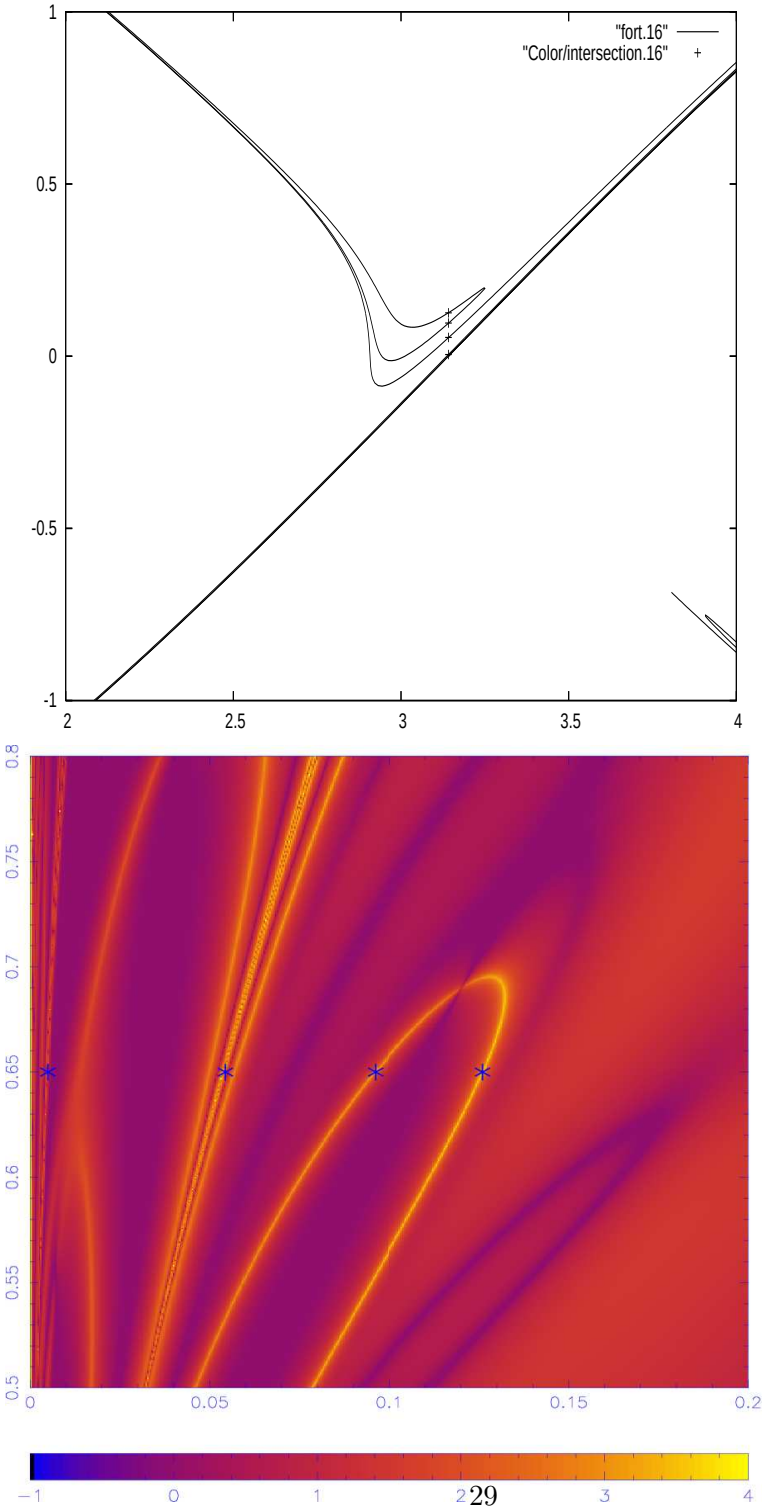

Figure 7: **On the top:** zoom of the unstable manifold around the hyperbolic fixed point obtained for $a_1 = a_2 = 1$, $\epsilon = 0.01$, $I_2(0) = 0.65$. The stars represent some intersection points of the manifold with the section $\varphi_1 = \pi$, which are then reproduced also on the bottom panel. **On the bottom:** Unstable manifold of Λ with the intersection points of the top panel.

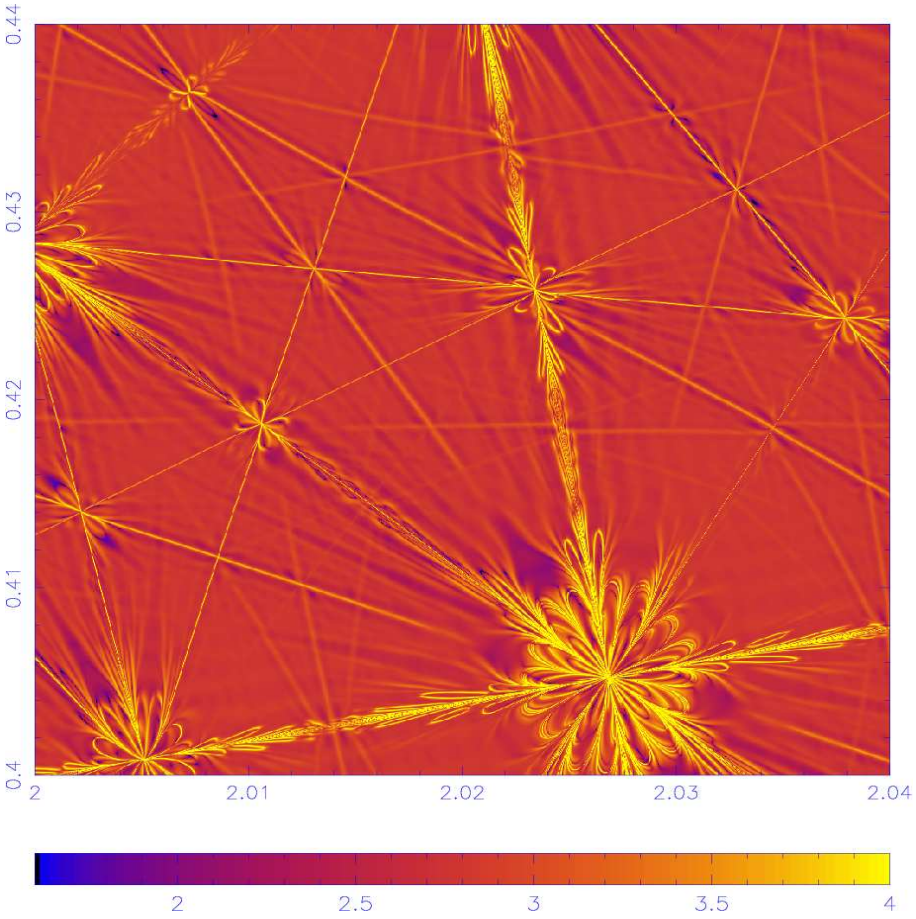

Figure 8: Detection of many of the flower–like structures for the map 2 computed for $\epsilon = 0.0001$.

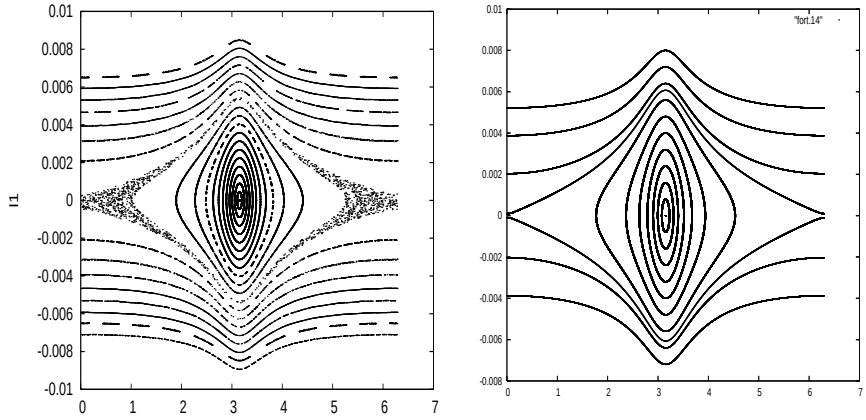

Figure 9: **Left:** Phase space portrait in the plane (I_1, φ_1) of a set of 40 orbits regularly spaced in $I_1(0)$ with $-0.008 < I_1(0) < 0.008$. The other initial conditions are $\varphi_1(0) = \pi$, $\varphi_2(0) = 0$, $I_2(0) = 0.397499949$. The points crossing the section $|\varphi_2| \leq 10^{-3}$ are plotted. As usual we can observe invariant KAM tori, libration islands and a chaotic orbit around the hyperbolic point at the origin. The perturbation parameter is $\epsilon = -10^{-5}$. **Right:** phase portrait of the main part the normal form (6), i.e. of the map generated by $I' \cdot \varphi + {I'_1}^2/2 + {I'_2}^2/2 + \epsilon u_0(\varphi_1)$. The most evident difference among the two phase portraits is the chaotic zone which appears around the hyperbolic point of the complete map (left panel), which is due to the remainder $\mathcal{R}$, i.e. the only part of the normal form which depends on φ_2.

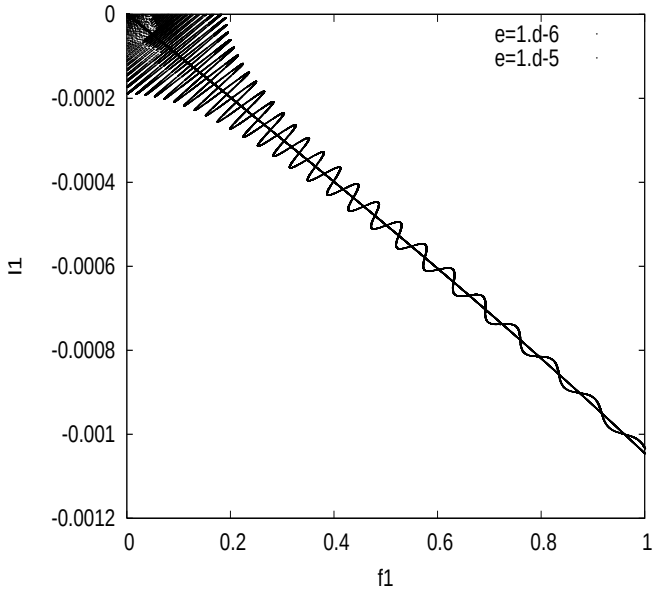
e=1.d-6
e=1.d-5
I1
f1
0
-0.0002
-0.0004
-0.0006
-0.0008
-0.001
-0.0012
0
0.2
0.4
0.6
0.8
1

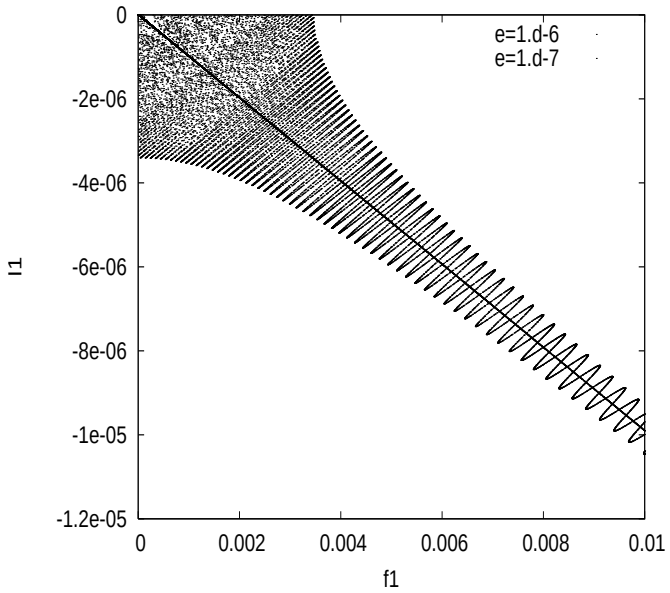
e=1.d-6
e=1.d-7
I1
f1
0
-2e-06
-4e-06
-6e-06
-8e-06
-1e-05
-1.2e-05
0
0.002
0.004
0.006
0.008
0.01

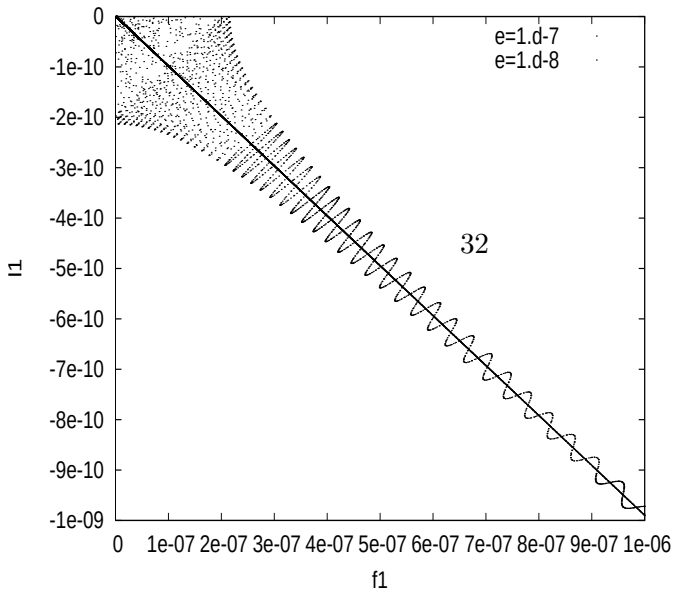
e=1.d-7
e=1.d-8
I1
f1
0
-1e-10
-2e-10
-3e-10
-4e-10
-5e-10
-6e-10
-7e-10
-8e-10
-9e-10
-1e-09
0
1e-07
2e-07
3e-07
4e-07
5e-07
6e-07
7e-07
8e-07
9e-07
1e-06

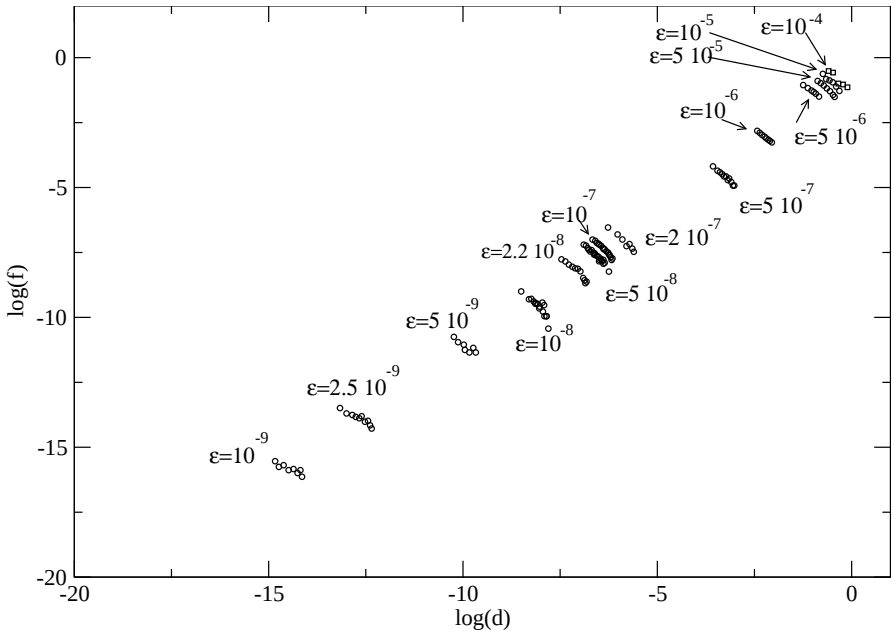

Figure 11: Variation of the size of the lobes as a function of the distance from the hyperbolic point $(0,0)$ for different values of ϵ going from -10^{-4} to -10^{-9}. Each set of data is well fitted by a power law : d^{m_ϵ}. The set of slopes m_ϵ has mean value $\bar{m} = -1.25$ and standard deviation $\sigma = 0.06$. The function $d^{\bar{m}}$ is a good fit of $f(d)$ in eq. 15.

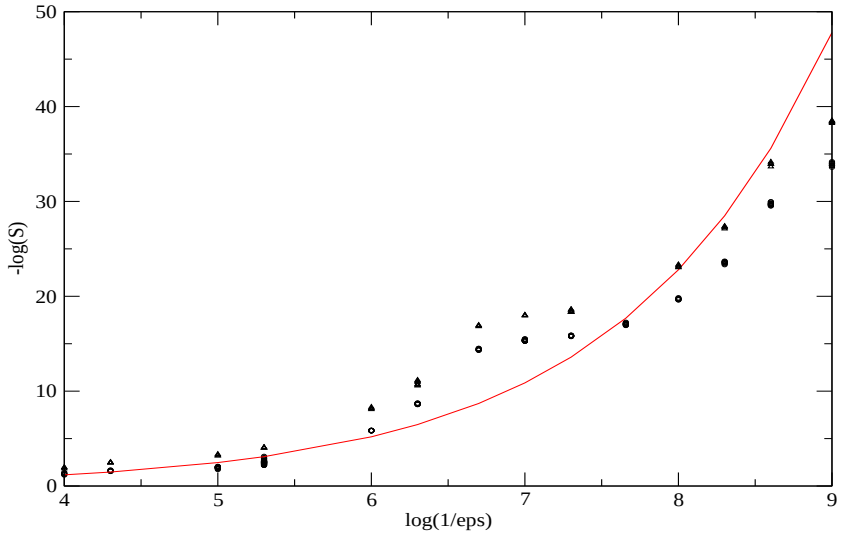

Figure 12: Variation of the normalized size of the lobes $S(\epsilon)$ as a function of $|\epsilon|$. The data are very well fitted by an exponential law as expected from eq. 15. Two different numerical experiments are reported: 1) measure of the size of the lobes (circle); 2) measure of the size of the chaotic region (triangle). We also plot a fit of data set 1 just to remark its exponential law.

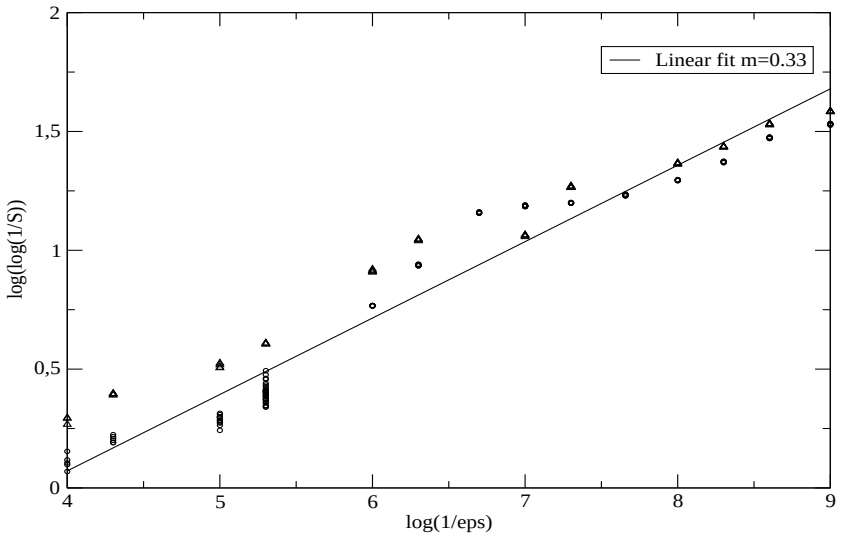

Figure 13: Same as figure 12 but taking the double logarithm of the size of the lobes. The data are well fitted by a linear law, as expected from eq. 15, with a slope of $\alpha = 0.33$.

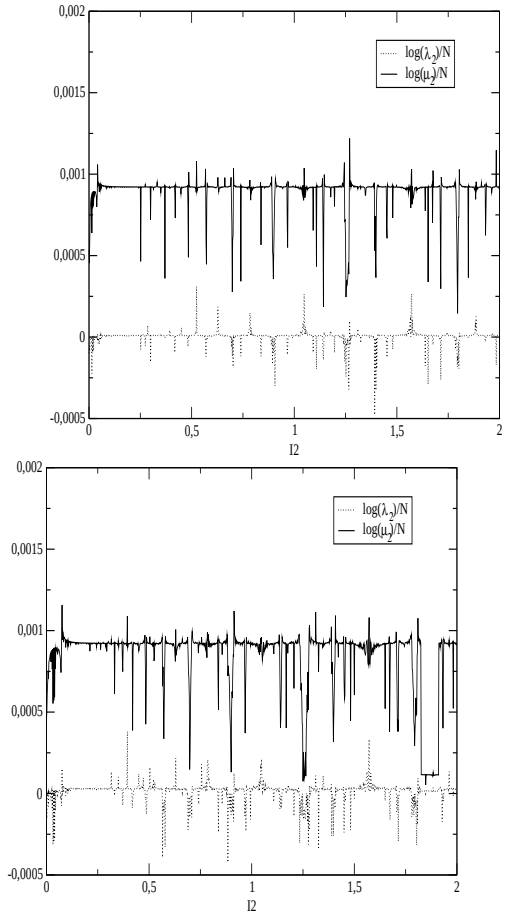

Figure 14: Numerical estimates of $\log \lambda_2/N$ and $\log \mu_2/N$, computed on a grid of 1000 initial conditions with $I_2 \in [0, 2]$, $I_1 = 0$, $\varphi_1 = \pi$, $\varphi_2 = 0$ and $\epsilon = 9\ 10^{-5}$ (on the left), $\epsilon = 3\ 10^{-4}$ (on the right).

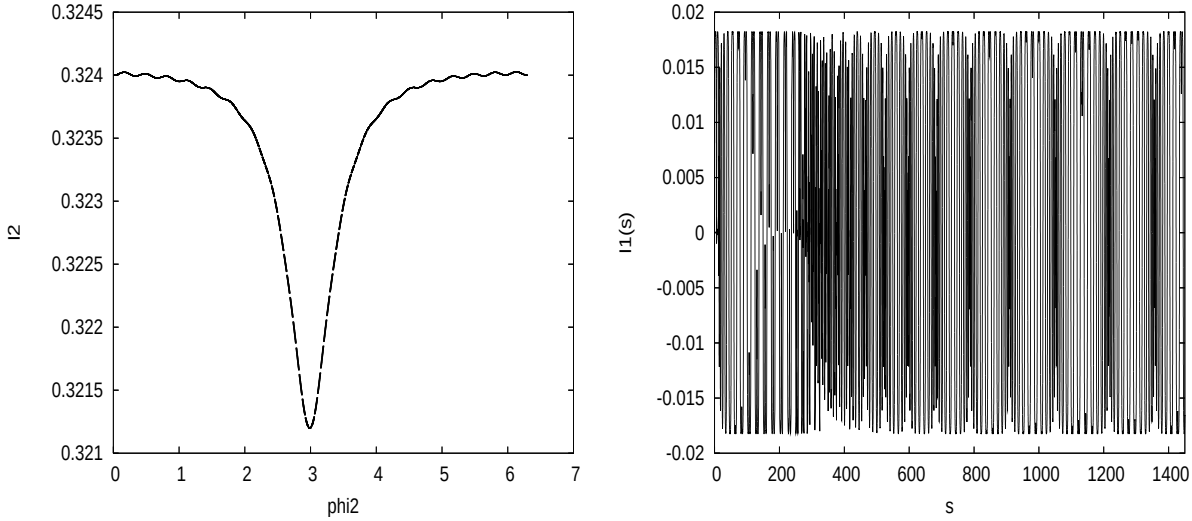

Figure 15: **On the left:** Representation of an orbit of the restricted map ($I_1 = 0$, $\varphi_1 = \pi$, $I_2 = 0.324$, $\varphi_2 = 0$) for $\epsilon = 9\,10^{-5}$. **On the right:** representation of $I_1(s)$ for that orbit.

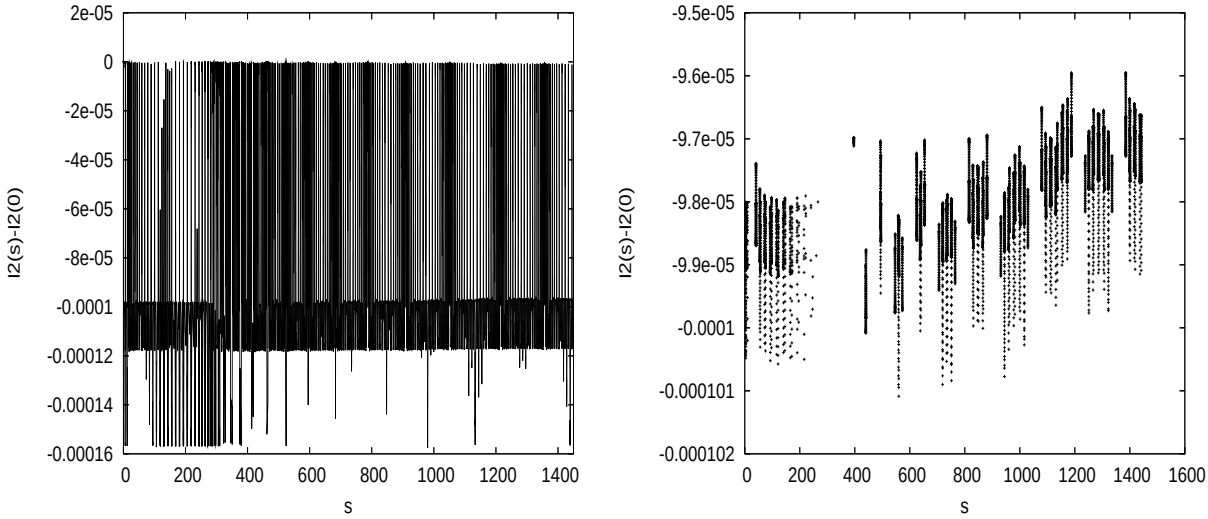

Figure 16: **On the left:** Representation of $I_2(s)$ for the orbit of the restricted map ($I_1 = 0$, $\varphi_1 = \pi$, $I_2 = 0.324$, $\varphi_2 = 0$) for $\epsilon = 9\,10^{-5}$. **On the right:** Representation of $I_2(s)$ for the same orbit but for a selected set of data having $-0.5 < \varphi_1 < 0.5$ and $I_1 > 0$. The large fluctuations on the left panel are mainly due to the excursion of I_2 as a function of φ_1. On the selected set (right) we appreciate the variation of I_2 due to the unrolling of the manifold along the I_2 axis.

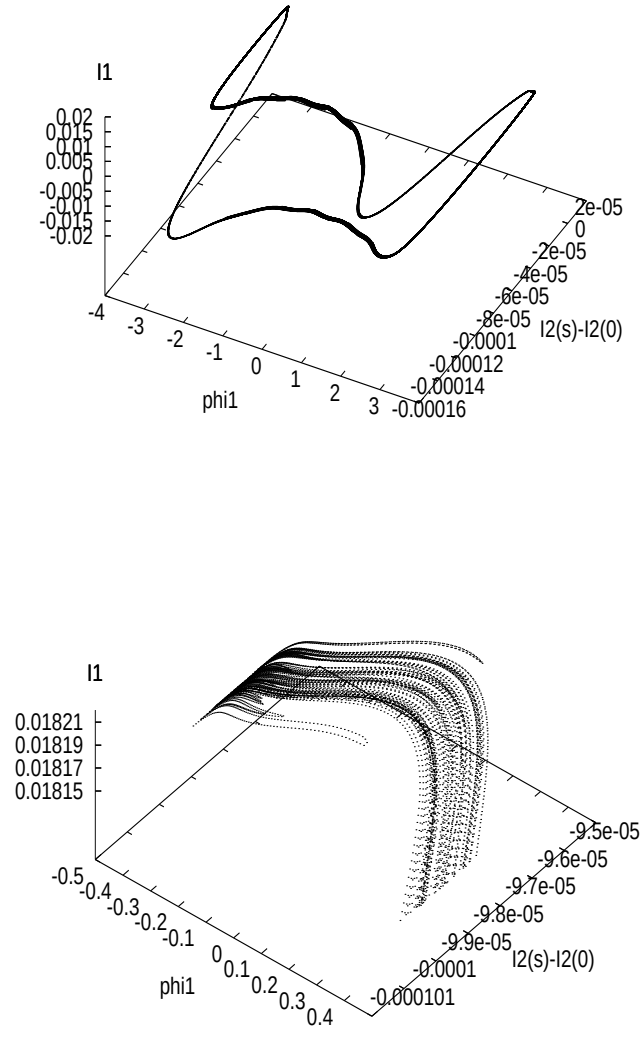

Figure 17: Representation of the unstable manifold of the orbit of figure 15 in the three dimensional space φ_1, I_2,I_1 (left panel). In order to appreciate the unrolling of the manifold in the I_2 direction we have plotted on the right panel a zoom of the manifold for values of $-0.5 < \varphi_1 < 0.5$ and $I_1 > 0$.

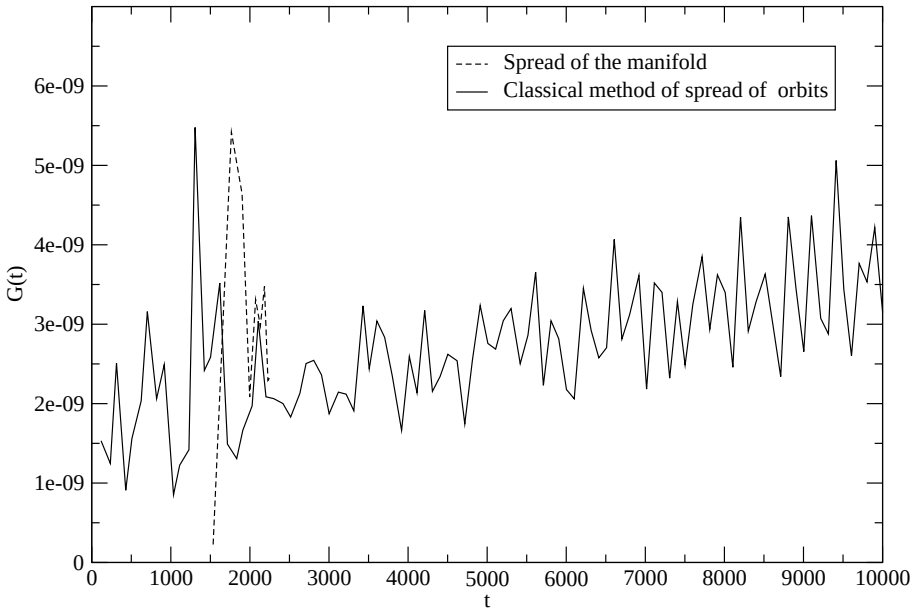

Figure 18: Evolution with time of the average of the mean squared distance from initial conditions for a set of 40 orbits with $I_1 = 0$, $\varphi_1 = \pi$, $0.3 < I_2 < 0.4$, $\varphi_2 = 0$ for $\epsilon = 3\,10^{-4}$.

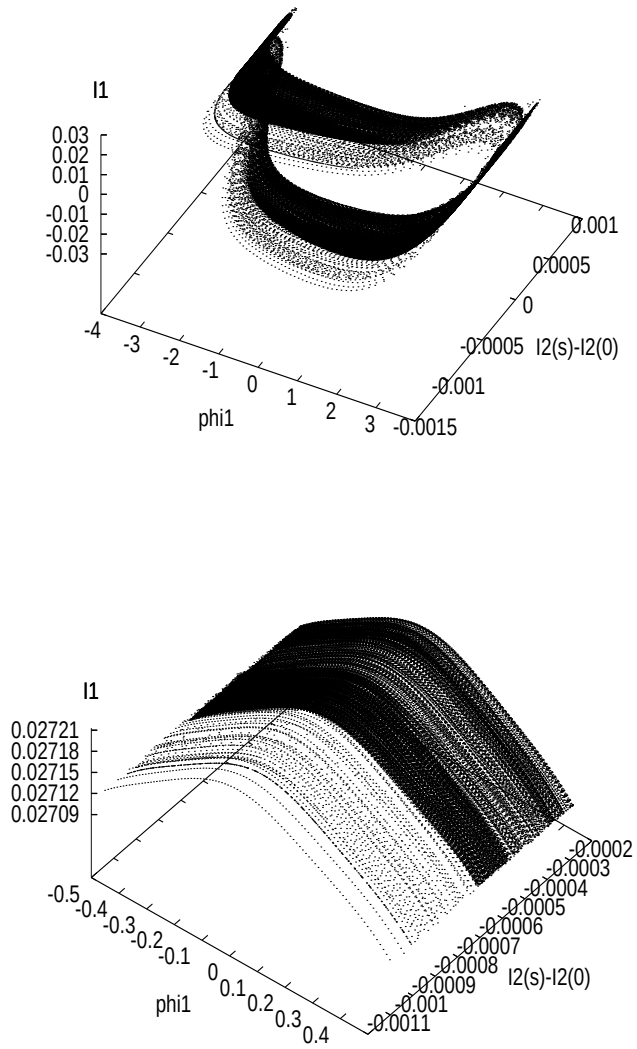

Figure 19: Representation of the unstable manifold of the orbit with initial condition $I_1 = 0$, $\varphi_1 = \pi$, $\varphi_2 = 0$, $I_2 = 0.324$ for $\epsilon = 2\,10^{-4}$ in the three dimensional space φ_1, I_2,I_1. Contrary to figure 17 we appreciate the unrolling of the manifold in the I_2 direction already on the global picture (left). For comparison with figure 17 we have plotted on the right panel a zoom of the manifold for values of $-0.5 < \varphi_1 < 0.5$ and $I_1 > 0$.